

AD-A012 297

COMPARISON OF COHERENT AND INCOHERENT BEAMFORMING
ENVELOPE DETECTORS FOR NORSAR REGIONAL SEISMIC EVENTS

Wen-Wu Shen

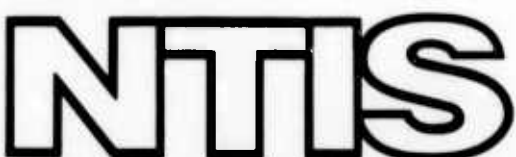
Texas Instruments, Incorporated

Prepared for:

Advanced Research Projects Agency
Air Force Technical Applications Center

31 December 1974

DISTRIBUTED BY:



National Technical Information Service
U. S. DEPARTMENT OF COMMERCE



APPROVED FOR PUBLIC RELEASE, DISTRIBUTION UNLIMITED

ALEX(01)-TR-74-06

205144

**COMPARISON OF COHERENT AND INCOHERENT BEAMFORMING ENVELOPE
DETECTORS FOR NORSAR REGIONAL SEISMIC EVENTS**

ADA012297

TECHNICAL REPORT NO. 6

VELA NETWORK EVALUATION AND AUTOMATIC PROCESSING RESEARCH

Prepared by
Wen-Wu Shen

TEXAS INSTRUMENTS INCORPORATED
Equipment Group
Post Office Box 6015
Dallas, Texas 75222

Prepared for
AIR FORCE TECHNICAL APPLICATIONS CENTER
Alexandria, Virginia 22314

Sponsored by
ADVANCED RESEARCH PROJECTS AGENCY
Nuclear Monitoring Research Office
ARPA Program Code No. 4F10
ARPA Order No. 2551

31 December 1974

Acknowledgment: This research was supported by the Advanced Research Projects Agency, Nuclear Monitoring Research Office, under Project VELA-UNIFORM, and accomplished under the technical direction of the Air Force Technical Applications Center under Contract No. F08606-74-C-0033.

UNCLASSIFIED

SECURITY CLASSIFICATION OF THIS PAGE (When Data Reduced)

REPORT DOCUMENTATION PAGE		READ INSTRUCTIONS BEFORE COMPLETING FORM
1. REPORT NUMBER	2. GOVT ACCESSION NO.	3. RECIPIENT'S CATALOG NUMBER
4. TITLE (and Subtitle) COMPARISON OF COHERENT AND INCOHERENT BEAMFORMING ENVELOPE DETECTORS FOR NORSAR REGIONAL SEISMIC EVENTS.		5. TYPE OF REPORT & PERIOD COVERED Technical
6. AUTHOR(s) Wen-Wu Shen		7. PERFORMING ORG. REPORT NUMBER ALEX(01)-TR-74-06
8. PERFORMING ORGANIZATION NAME AND ADDRESS Texas Instruments Incorporated Equipment Group Dallas, Texas 75222		9. CONTRACT OR GRANT NUMBER(s) F08606-74-C-0033
10. PROGRAM ELEMENT, PROJECT, TASK AREA & WORK UNIT NUMBERS VELA T/4705/B/ETR		11. CONTROLLING OFFICE NAME AND ADDRESS Advanced Research Projects Agency Nuclear Monitoring Research Office Arlington, Virginia 22209
12. REPORT DATE 31 December 1974		13. NUMBER OF PAGES 82
14. DISTRIBUTION STATEMENT (if this report is different from Controlling Office) Air Force Technical Applications Center VELA Seismological Center Alexandria, Virginia 22314		15. SECURITY CLASS. (of this report) UNCLASSIFIED
16. DISTRIBUTION STATEMENT (of the abstract entered in Block 20, if different from Report)		17. DECLASSIFICATION/DOWNGRADING SCHEDULE
18. SUPPLEMENTARY NOTES ARPA Order No. 2551		
19. KEY WORDS (Continue on reverse side if necessary and identify by block number) Seismology Seismic Array Coherent and Incoherent Beams Envelope Detectors Hilbert Transform, False Alarm and Detection Probabilities Detector Operating Characteristics		
20. ABSTRACT (Continue on reverse side if necessary and identify by block number) The performance of the conventional coherent beam envelope detector and the incoherent beam envelope detector were studied and compared using short-period Norwegian Seismic Array (NORSAR) data from regional earthquakes and presumed explosions. The detectors were evaluated in two frequency bands in terms of detection performance, false alarm characteristic, and the resultant operating characteristic. A detector using the		

DD FORM 1 JAN 68 1A73 EDITION OF 1 NOV 65 IS OBSOLETE

UNCLASSIFIED

SECURITY CLASSIFICATION OF THIS PAGE WHEN DRAFTED

UNCLASSIFIED

SECURITY CLASSIFICATION OF THIS PAGE(When Data Entered)

20. Continued

envelope of the array beam computed with the Hilbert transform was also examined.

UNCLASSIFIED

SECURITY CLASSIFICATION OF THIS PAGE(When Data Entered)

ABSTRACT

The performances of the conventional coherent beam envelope detector and the incoherent beam envelope detector were studied and compared using short-period Norwegian Seismic Array (NORSAR) data from regional earthquakes and presumed explosions. The detectors were evaluated in two frequency bands in terms of detection performance, false alarm characteristic, and the resultant operating characteristic. On the basis of the derived operating characteristics from data, the detectors with specific operating pass-band are ranked in the capability-decreasing order: incoherent detector (1.5-2.5 Hz), coherent detector (1.5-2.5 Hz), incoherent detector (3.0-4.0 Hz), and coherent detector (3.0-4.0 Hz). A detector using the envelope of the array beam computed with the Hilbert transform was also examined.

Neither the Advanced Research Projects Agency nor the Air Force Technical Applications Center will be responsible for information contained herein which has been supplied by other organizations or contractors, and this document is subject to later revision as may be necessary. The views and conclusions presented are those of the authors and should not be interpreted as necessarily representing the official policies, either expressed or implied, of the Advanced Research Projects Agency, the Air Force Technical Applications Center, or the US Government.

ACKNOWLEDGMENTS

Several people have contributed in various ways to the completion of this report. I wish to thank Lt. R. W. Alewine, Lt. M. J. Marcus, and Messrs. T. E. Barnard, T. W. Harley, F. Ringdal, R. L. Sax, and W. H. Swindell who provided technical suggestions and discussions in the course of this work.

I also wish to thank Mrs. Cherylann Saunders who typed and edited the manuscript, Mr. James Battis for drafting the figures, and Messrs. W. H. Swindell and T. E. Barnard who patiently extended their guidance and suggestions in editing and writing this report.

TABLE OF CONTENTS

SECTION	TITLE	PAGE
	ABSTRACT	iii
	ACKNOWLEDGEMENTS	iv
I.	INTRODUCTION	I-1
II.	THE DETECTION ALGORITHMS AND THE FUNDAMENTALS OF FALSE ALARM AND DETECTION PROBABILITIES	II-1
A.	INTRODUCTION	II-1
B.	COHERENT AND INCOHERENT BEAMFORMING	II-1
C.	THE ENVELOPES	II-2
D.	THE DETECTOR OUTPUT	II-6
E.	FALSE ALARM PROBABILITY	II-7
F.	DETECTION PROBABILITY	II-8
G.	DETECTOR OPERATING CHARACTERISTIC	II-9
III.	DATA BASE	III-1
IV.	RESULTS AND DISCUSSIONS	IV-1
A.	INTRODUCTION	IV-1
B.	ILLUSTRATION OF COMPUTATION	IV-1
C.	THE MEASURED FALSE ALARM PROBABILITY	IV-4
D.	DETECTION PERFORMANCE	IV-19
E.	THE MEASURED DETECTOR OPERATING CHARACTERISTICS	IV-40

TABLE OF CONTENTS
(continued)

SECTION	TITLE	PAGE
V.	CONCLUSIONS	V-1
	A. FALSE ALARM RATE MEASUREMENTS	V-1
	B. DETECTOR PERFORMANCE	V-2
	C. DETECTOR OPERATING CHARACTERISTICS	V-3
VI.	REFERENCES	VI-1

LIST OF FIGURES

FIGURE	TITLE	PAGE
II-1	RESPONSE OF 1.5-2.5 Hz AND 3.0-4.0 Hz FILTERS	II-3
IV-1	AN ILLUSTRATION OF ARRAY BEAMS, STAS AND LTAS (KAZ/282/06N, 1.5-2.5 Hz)	IV-2
IV-2	AN ILLUSTRATION OF ARRAY BEAMS, STAS, LTAS (DAY 214 OF 1971 NOISE, 1.5-2.5 Hz)	IV-3
IV-3	AN ILLUSTRATION OF ARRAY BEAMS, ENVELOPES AND LTAS USING HILBERT TRANSFORM (KAZ/282/06N, 1.5-2.5 Hz)	IV-5
IV-4	AN ILLUSTRATION OF ARRAY BEAMS, ENVELOPES, AND LTAS USING HILBERT TRANSFORM (DAY 214 OF 1971 NOISE, 1.5-2.5 Hz)	IV-6
IV-5	AN ILLUSTRATION OF DETECTOR OUTPUT, SNR (KAZ/282/06N, 1.5-2.5 Hz)	IV-7
IV-6	AN ILLUSTRATION OF DETECTOR OUTPUT, SNR (DAY 214 1971 NOISE, 1.5-2.5 Hz)	IV-8
IV-7	AN ILLUSTRATION OF DETECTOR OUTPUT USING HILBERT TRANSFORM (KAZ/282/06N, 1.5-2.5 Hz)	IV-9
IV-8	AN ILLUSTRATION OF DETECTOR OUTPUT USING HILBERT TRANSFORM (DAY 214 1971 NOISE, 1.5-2.5 Hz)	IV-10
IV-9	FALSE ALARM HISTOGRAM FOR AN INCOHERENT DETECTOR (DAY 214 OF 1971 NOISE, 1.5-2.5 Hz)	IV-11
IV-10	FALSE ALARM PROBABILITY FOR ADJUSTED-DELAY BEAM IN THE 1.5-2.5 Hz PASSBAND (FROM TEN NOISE SAMPLES)	IV-13

LIST OF FIGURES
(continued)

FIGURE	TITLE	PAGE
IV-11	FALSE ALARM PROBABILITY FOR ADJUSTED-DELAY BEAM IN THE 3.0-4.0 Hz PASSBAND (FROM TEN NOISE SAMPLES)	IV-14
IV-12	FALSE ALARM PROBABILITY FOR DIVERSITY-STACK BEAM IN THE 1.5-2.5 Hz PASSBAND (FROM TEN NOISE SAMPLES)	IV-15
IV-13	FALSE ALARM PROBABILITY FOR DIVERSITY-STACK BEAMS IN THE 3.0-4.0 Hz PASSBAND (FROM TEN NOISE SAMPLES)	IV-16
IV-14	COHERENT ADJUSTED-DELAY DETECTOR OUTPUT VERSUS INCOHERENT DETECTOR OUTPUT $((STA/LTA)_{max})$ IN THE 1.5-2.5 Hz PASSBAND)	IV-20
IV-15	COHERENT DIVERSITY-STACK DETECTOR OUTPUT VERSUS INCOHERENT DETECTOR OUTPUT $((STA/LTA)_{max})$ IN THE 1.5-2.5 Hz PASSBAND)	IV-21
IV-16	COHERENT ADJUSTED-DELAY DETECTOR OUTPUT VERSUS INCOHERENT DETECTOR OUTPUT $((STA)_{max}/LTA)$ IN THE 1.5-2.5 Hz PASSBAND)	IV-22
IV-17	COHERENT DIVERSITY-STACK DETECTOR OUTPUT VERSUS INCOHERENT DETECTOR OUTPUT $((STA)_{max}/LTA)$ IN THE 1.5-2.5 Hz PASSBAND)	IV-23
IV-18	COHERENT ADJUSTED-DELAY DETECTOR OUTPUT VERSUS INCOHERENT DETECTOR OUTPUT $((STA/LTA)_{max})$ IN THE 3.0-4.0 Hz PASSBAND)	IV-24
IV-19	COHERENT DIVERSITY-STACK DETECTOR OUTPUT VERSUS INCOHERENT DETECTOR OUTPUT $((STA/LTA)_{max})$ IN THE 3.0-4.0 Hz PASSBAND)	IV-25

LIST OF FIGURES
(continued)

FIGURE	TITLE	PAGE
IV-20	COHERENT ADJUSTED-DELAY DETECTOR OUTPUT VERSUS INCOHERENT DETECTOR OUTPUT ($(STA)_{max}/LTA$ IN THE 3.0-4.0 Hz PASSBAND)	IV-26
IV-21	COHERENT DIVERSITY-STACK DETECTOR OUTPUT VERSUS INCOHERENT DETECTOR OUTPUT ($(STA)_{max}/LTA$ IN THE 3.0-4.0 Hz PASSBAND)	IV-27
IV-22	MEAN SUBARRAY SNR VERSUS DETECTOR OUTPUT (KAZ/282/06N)	IV-32
IV-23	MEAN SUBARRAY SNR VERSUS DETECTOR OUTPUT (WRS/248/07N)	IV-34
IV-24	DETECTION PROBABILITY FROM 91 EVENTS $(STA/LTA)_{max}$ IN 1.5-2.5 Hz PASSBAND	IV-36
IV-25	DETECTION PROBABILITY FROM 91 EVENTS $(STA/LTA)_{max}$ IN 3.0-4.0 Hz PASSBAND	IV-37
IV-26	DETECTION PROBABILITY FROM 91 EVENTS $(STA)_{max}/LTA$ in 1.5-2.5 Hz PASSBAND	IV-38
IV-27	DETECTION PROBABILITY FROM 91 EVENTS $(STA)_{max}/LTA$ in 3.0-4.0 Hz PASSBAND	IV-39
IV-28	DETECTOR OPERATING CHARACTERISTICS (DIVERSITY-STACK BEAMS $(STA/LTA)_{max}$ MODE)	IV-42
IV-29	DETECTOR OPERATING CHARACTERISTICS (DIVERSITY-STACK BEAMS $(STA)_{max}/LTA$ MODE)	IV-44

LIST OF TABLES

TABLE	TITLE	PAGE
III-1	EVENT INFORMATION	III-2
III-2	DETECTOR OUTPUT (dB) (1.5-2.5 Hz BAND)	III-4
III-3	NOISE SAMPLES	III-8
IV-1	STATISTICAL PARAMETERS DERIVED FROM FIGURES IV-10 THROUGH IV-13	IV-18
IV-2	AVERAGES OF DETECTOR OUTPUT FOR EVENT ENSEMBLE	IV-29
IV-3	DETECTOR OUTPUT USING HILBERT TRANSFORMATION	IV-30

SECTION I INTRODUCTION

This report presents the results of a study of detection on the envelope of short-period array beams from the Norwegian Seismic Array (NORSAR) which had been formed through either incoherent summation or conventional coherent summation techniques. Coherent beamforming of a large short-period array does not yield the theoretically predicted signal-to-noise ratio improvement due to imperfect signal similarity across the array. This signal dissimilarity is frequency dependent with the most pronounced drop in signal coherence occurring at frequencies above 2Hz. Thus, high frequency signals suffer the largest losses in signal-to-noise ratio (SNR). At NORSAR, this type of signal originates from near-regional events and Eurasian presumed explosions, particularly those from Western Russia (Ringdal et al., 1972).

Signal loss also may occur even with well-equalized and similar signal waveforms if the regional corrections are not known or if the signal arrives slightly off-azimuth from the direction of a preformed beam. Whenever signal dissimilarity is severe enough to cause appreciable loss in signal-to-noise ratio during conventional coherent beam forming or when beaming parameters are in slight error, incoherent beamforming using the sum of the rectified sensor or subarray output may allow partial recovery of the signal loss.

The objective of this study was to investigate systematically the performance of the envelope detector in detecting underground explosions and near-regional earthquakes. The following steps were undertaken to accomplish this objective:

- Measuring the false alarm probability of coherent and incoherent envelope detectors.
- Computing the detection probability of coherent and incoherent envelope detectors for presumed underground explosions and near-regional earthquakes.
- Comparing the operating characteristics of the detectors.

Section II describes the detection algorithms and the mathematical basis of the false alarm and detection probabilities. Section III describes the data base. Section IV discusses the results of this study. Finally, a concluding summary is made in the last section.

SECTION II

THE DETECTION ALGORITHMS AND THE FUNDAMENTALS OF FALSE ALARM AND DETECTION PROBABILITIES

A. INTRODUCTION

This section describes the mathematical operations of the detection system and the general concept of false alarm and detection probabilities used in evaluating detection performance. The coherent and incoherent array beamformers are described in Subsection B, followed by a description of envelope forming in Subsection C. Subsection D describes the detector output. The last three subsections introduce the fundamentals of false alarm and detection probabilities, and detector operating characteristics, respectively.

B. COHERENT AND INCOHERENT BEAMFORMING

Let $S_i(t)$ be the time trace of subarray i . The conventional coherent beam is defined as

$$AB_C(t) = \frac{1}{N} \sum_{i=1}^N S_i(t - \tau_i) \quad (\text{II-1})$$

where $AB_C(t)$ is the coherent array beam, τ_i is the travel-time delay of the signal waveform for subarray i and N is the number of channels.

Following Ringdal et al., (1972), the incoherent array beam, $AB_I(t)$, was formed by summing the absolute values of the subarray beams:

$$AB_I(t) = \frac{1}{N} \sum_{i=1}^N |S_i(t - \tau_i)| \quad (\text{II-2})$$

where the symbols used here have the same meaning as in equation (II-1).

In the work described here, each channel, (i.e., subarray beam $S_i(t)$), was prefiltered with a zero-phase bandpass filter before forming the array beam. To compare detector performance in different frequency ranges, two passbands, 1.5-2.5 Hz and 3.0-4.0 Hz, were used. Both sides of each passband were given a 0.7 Hz-wide cosine taper. Figure II-1 shows the filter amplitude response for the two passbands.

Both adjusted-delay and diversity-stack techniques were used for array beamforming. The travel time delay τ_i for each channel appropriate for each signal was computed either from the cross correlation function with a reference channel or from manual input. For adjusted-delay beamforming, each channel is equally weighted; for diversity-stack beamforming, each channel was weighted by the quantity $W(i)$ which was computed according to the formula (Texas Instruments, 1971):

$$W(i) = \sqrt{\frac{P_s(i) - P_n(i)}{P_n(i)}} \quad (II-3)$$

where $P_s(i)$ and $P_n(i)$ are signal and noise powers for channel i , respectively.

C. THE ENVELOPES

1. Short-Term-Averages As Envelopes

The envelopes of the coherent and incoherent array beams $AB_C(t)$ and $AB_I(t)$ defined by equations (II-1) and (II-2) were formed by taking a running average over a specified gate length:

$$STA(t) = \frac{1}{L+1} \sum_{\ell=0}^L |AB(t - \ell\Delta t)| \quad (II-4)$$

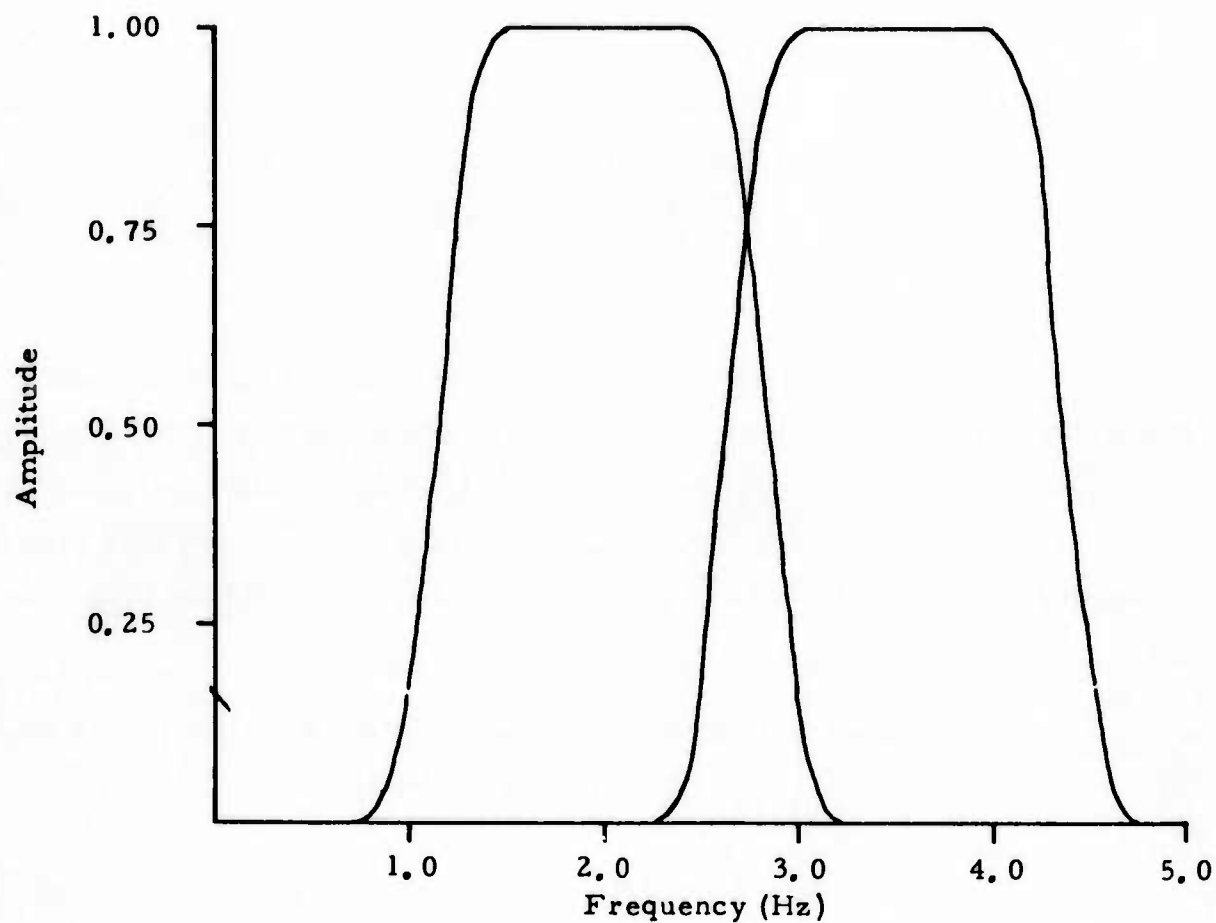


FIGURE II-1
RESPONSE OF 1.5-2.5 Hz AND
3.0-4.0 Hz FILTERS

where STA refers to short-term-averages and is used to represent the envelope amplitude of signals, Δt is the sample interval and $L+1$ is the number of points averaged. For the short-period NORSAR data processed, Δt was 0.1 seconds and $L+1$ was set to 15, equivalent to 1.5 seconds, which is the timegate used in the NORSAR on-line detection system.

The STA envelope is fast and straightforward to compute; however, strictly speaking, it is only an approximation of the envelope of a signal wave train. The envelope of a time series is defined by the magnitude of its analytic function computed from its Hilbert transform.

2. Amplitudes of Analytical Signal As Envelopes

Since the short-term-average represents only the approximate shape of a wave train envelope, the maximum amplitude of a signal is not accurately measured in the STA representation. Because the true envelope amplitude may allow better bodywave magnitude measurements and may also increase the detectability of event signals, an attempt was made to form the exact envelope of a wave train by Hilbert transformation.

The Hilbert transform of a time series $x(t)$ is the time series $\hat{x}(t)$ defined by the convolution integral (Cizek, 1970):

$$\hat{x}(t) = -\frac{1}{\pi} \int_{-\infty}^{\infty} \frac{x(\tau)}{\tau - t} d\tau = -\frac{1}{\pi t} * x(t). \quad (\text{II-5})$$

Denoting $X(f)$ as the Fourier transform of $x(t)$ and $H(f)$ as that of $(-\frac{1}{\pi t})$, we have

$$F\left\{\hat{x}(t)\right\} = X(f) \cdot H(f) \quad (\text{II-6})$$

where

$$H(f) = \begin{cases} -j & \text{if } f < 0 \\ 0 & \text{if } f = 0 \\ +j & \text{if } f > 0 \end{cases}$$

and $j = \sqrt{-1}$.

To compute equation (II-5) in discrete form, let x_i , $i = 0, 1, \dots, M-1$, denote the sequence of M complex finite values of $x(t)$. Then the discrete Fourier transform (DFT) of this sequence is a sequence X_k , $k=0, 1, \dots, M-1$, defined by

$$X_k = \frac{1}{M} \sum_{i=0}^{M-1} x_i e^{-jik(2\pi/M)}. \quad (\text{II-7})$$

For an inverse DFT, the sequence x_i is defined by

$$x_i = \sum_{k=0}^{M-1} X_k e^{+jik(2\pi/M)}. \quad (\text{II-8})$$

Equation (II-5) holds true for the Fourier transform of a Hilbert transform. Therefore, the discrete Hilbert transform can be performed in the frequency domain through Fourier transformation. In doing so, let G_k be the sequence of equation (II-6):

$$G_k = X_k \cdot H_k \quad (\text{II-9})$$

where

$$H_k = \begin{cases} -j & \text{if } k = 1, 2, \dots, \frac{M}{2} - 1 \\ 0 & \text{if } k = 0, M/2 \\ +j & \text{if } k = \frac{M}{2} + 1, \dots, M-1 \end{cases}$$

The discrete sequence of the process $\hat{x}(t)$ is obtained from the inverse DFT of the sequence G_k in equation (II-9).

Define the complex process $z(t)$ by taking

$$z(t) = x(t) + j\hat{x}(t). \quad (\text{II-10})$$

This process is known as the analytic signal associated with $x(t)$. Finally, the envelope of $x(t)$ is the amplitude of $z(t)$ (Bracewell, 1965) which is

$$E(t) = \left[x^2(t) + \hat{x}^2(t) \right]^{1/2}. \quad (\text{II-11})$$

For coherent array beamforming, $x(t)$ in equation (II-11) is obtained from $AB_C(t)$ in equation (II-1). The incoherent array envelope $E_I(t)$ was formed by averaging the subarray envelopes:

$$E_I(t) = \frac{1}{N} \sum_{i=1}^N E_i(t - \tau_i) \quad (\text{II-12})$$

where

E_i is the envelope of subarray i ,

τ_i is the wave travel-time delay, and

N is the number of subarrays.

D. THE DETECTOR OUTPUT

In the decision-making process of a detection system, the estimated signal-to-noise ratio (SNR) commonly is used as the detection statistic. A detection is declared when the SNR exceeds a preselected decision threshold. Here, signal levels were measured by the quantities STA and E. For operational detectors, the conventional computation of noise RMS values is somewhat tedious and is difficult to realize in practice. Thus the Long-Term-Averages (LTA) was introduced to represent the noise level. The LTA is computed in the same manner as in equation (II-4), but with an integration time of 30 seconds. Because the LTA is averaged over a much longer time window than the STA, it is a good approximation of the noise mean value. The signal-to-noise ratio (expressed in dB) for the detection system used here was thereafter denoted by

$$\text{SNR}(t) = 20 \times \log_{10} (\text{STA}(t) / \text{LTA}(t)) \quad (\text{II-13})$$

STA must be replaced with E(t) for the envelope computed from the Hilbert transform.

The process in equation (II-13) was the actual operational mode in event detection. However, the running LTA(t) was contaminated with signal energy when maximum SNR(t) occurred. To obtain a more meaningful estimate of the signal-to-noise ratio, the LTA was frozen prior to the signal arrival, the time of which was determined from the event location and origin time. The maximum amplitude of the envelope in a signal gate was used for the computation of signal-to-noise ratio:

$$\text{SNR} = 20 \times \log_{10} ((\text{STA})_{\max} / \overline{\text{LTA}}) \quad (\text{II-14})$$

where STA is replaced with E if the analytic signal is used, and where $\overline{\text{LTA}}$ is the average of LTA in the noise gate. Both processes of equations (II-13) and (II-14) were performed.

E. FALSE ALARM PROBABILITY

When a detector output exceeds the decision threshold while there is no signal present, it is a false alarm known as Type I Error in the detection problem. False alarm probability can be measured by forming the histogram of detector output in noise. This normalized histogram is essentially the false alarm probability density function for the detection system. If the noise amplitudes are log normally distributed, the probability density function follows a Gaussian distribution:

$$\frac{dF}{dS} = P_f(S) = \frac{1}{\sqrt{2\pi} \sigma_n} \exp \left[-\frac{1}{2} \left(\frac{S - \mu_n}{\sigma_n} \right)^2 \right] \quad (\text{II-15})$$

where

- S is the detector output for noise,
- μ_n is the mean value, and
- σ_n is the standard deviation.

Thus, dF/dS or $P_f(S)$ is the false alarm probability density function.

False alarm probability for a given decision threshold S^* is obtained by integrating the density function from S^* to infinity, or, mathematically

$$F = \int_{S^*}^{\infty} P_f(S) dS. \quad (\text{II-16})$$

This cumulative distribution function can be used to determine the probable number of false alarms registered by the detector for a given time period.

F. DETECTION PROBABILITY

When the detector fails to detect a signal for various reasons such as signal dissimilarity, erroneous look direction, or weak events, the failure is called a Type II Error. Assuming the signal amplitude to be a random variable the probability of detecting a signal at a given level is called the detection probability for that level.

If the signal amplitude is log normally distributed, the probability density function of the output level follows a Gaussian distribution:

$$\frac{dD}{dS} = P_d(S) = \frac{1}{\sqrt{2\pi} \sigma_s} \exp \left[-\frac{1}{2} \left(\frac{S - \mu_s}{\sigma_s} \right)^2 \right] \quad (\text{II-17})$$

as its cumulative function from S^* to infinity

$$D = \int_{S^*}^{\infty} P_d(S) dS \quad (\text{II-18})$$

is thus the probability of detection at the decision threshold S^* .

Experimentally, the detection probability density function is obtained by forming the histogram for the detector output from events and the detection probability by integrating the density function from a given level to infinity.

G. DETECTOR OPERATING CHARACTERISTIC

From the false alarm probability, $F(S)$, and the detection probability, $D(S)$ of a given detector, the common factor S can be eliminated to form a new function $S(F, D)$ which is known as the Detector Operating Characteristic or Detector Operating Curve.

The operating curve is a display of detection probability versus the false alarm probability for a given detector-output level (SNR). For various detectors, this display enables us to evaluate the relative detector performance by comparing the detection probabilities for a given false alarm rate or the false alarm rates for a given detection probability. The detector curves derived from the data will be shown in Subsection IV-E.

SECTION III DATA BASE

The data used in this report were NORSAR short-period subarray beams of near-regional earthquakes and presumed underground explosions which had been formed during a previous short-period NORSAR array evaluation program (Barnard and Whitelaw, 1972; Ringdal and Whitelaw, 1973). The available data for this purpose were very much limited. In order to obtain a more reliable statistical analysis, all earthquakes with epicentral distance less than twenty-seven degrees and all presumed underground explosions which were available on existing subarray beam tapes were processed. In all, there were 55 earthquakes and 36 presumed explosions which were used. Table III-1 lists the bodywave magnitude, location, depth, epicentral delta and source time of these events. In the table, the first three characters of event identification indicate the seismic region of an event. The middle three-digit number indicates the Julian day and the last two-digit number indicates the hour of event time. The other symbols or characters are only for convenience in processing. The distribution of the earthquake magnitude is relatively narrow and is not representative of the general seismicity. The magnitude distribution of the presumed explosion is even more narrowly restricted and essentially does not overlap the earthquake distribution. Therefore, the m_b -values distribution for the ensemble is not statistically well-behaved.

The detector output signal-to-noise ratios for both adjusted delay and diversity-stack beams are tabulated in Table III-2. Both the updated LTA, $(STA/LTA)_{max}$ and the averaged LTA, $(STA)_{max}/\overline{LTA}$ are shown in two passbands.

The false alarm probability was calculated for ten noise samples each 320 seconds long. Table III-3 describes these samples.

TABLE III-1

EVENT INFORMATION
(PAGE 1 OF 2)

Event I.D.	m_b	Lat.	Long.	Depth	Δ	Day	Time
NZM/241/05N	6.3	73.3N	55.1E	0.0	20.5	09/28/72	05.59.57
NZM/270/06N	6.4	73.4N	55.1E	0.0	20.5	09/27/71	05.59.55
SWR/277/08N	5.8	46.8N	45.0E	0.0	24.1	10/08/72	08.59.58
URA/082/06N	5.6	61.3N	56.5E	0.0	21.6	03/23/71	06.59.56
KAZ/356/06N	6.0	47.9N	48.2E	0.0	24.8	12/22/71	06.59.56
URA/191/16N	5.3	64.2N	55.2E	0.0	20.3	07/10/71	16.59.59
JAP/063/07N	5.2	40.7N	143.5E	0.0	71.4	03/04/71	07.48.39
KUR/142/12N	3.8	49.0N	154.0E	0.0	66.2	05/22/71	12.59.53
CAN/310/22N	6.8	51.5N	179.1E	2.0	67.3	11/06/71	22.00.00
TAD/188/04N	4.5	38.6N	73.1E	0.0	43.8	07/07/71	03.52.53
IRA/102/19N1	6.0	28.3N	55.6E	0.0	44.1	04/12/71	19.03.26
KUR/077/03N	5.1	49.2N	156.3E	0.0	66.5	03/18/71	03.13.15
KM1/073/12N	5.3	53.9N	160.5E	0.0	62.9	03/14/71	12.15.14
NEV/230/14N	5.4	37.1N	116.0W	0.0	72.9	08/18/71	14.00.00
KAZ/070/04N	5.5	49.8N	78.2E	0.0	38.0	03/10/72	04.56.57
EKZ/363/04N	4.5	50.0N	78.0E	0.0	37.8	12/28/72	04.26.58
EK2/345/04N	6.0	50.1N	78.8E	0.0	38.1	12/10/72	04.27.08
EK1/345/04N	5.7	49.8N	78.1E	0.0	38.0	12/10/72	04.26.58
EKZ/246/08N	5.1	50.0N	77.7E	0.0	37.6	09/02/72	08.56.58
EKZ/239/03N	5.5	50.0N	77.8E	0.0	37.7	08/26/72	03.46.57
EKZ/229/03N	5.2	49.8N	78.1E	0.0	38.0	08/16/72	03.16.57
EKZ/188/01N	4.4	49.7N	78.0E	0.0	38.0	07/06/72	01.02.58
EKZ/041/05N	5.5	50.0N	78.9E	0.0	38.2	02/10/72	05.02.57
EKZ/364/06N	5.8	49.7N	78.1E	0.0	38.0	12/30/71	06.20.58
EKZ/349/07N	4.9	50.0N	77.9E	0.0	37.7	12/15/71	07.52.59
EKZ/333/06N	5.5	49.8N	78.1E	0.0	38.0	11/29/71	06.02.57
EKZ/294/06N	5.6	50.0N	77.6E	0.0	37.6	10/21/71	06.02.57
EKZ/159/01N	5.5	49.8N	78.2E	0.0	38.0	06/07/72	01.27.57
KAZ/181/04N	5.4	50.0N	79.1E	0.0	38.0	06/30/71	03.56.57
KAZ/282/06N	5.4	50.0N	77.7E	0.0	37.6	10/09/71	06.02.57
KAZ/157/04N	5.5	50.0N	77.8E	0.0	37.7	06/06/71	04.02.57
KAZ/145/04N	5.2	49.8N	78.2E	0.0	38.0	05/25/71	04.02.58
KAZ/115/03N	5.9	49.8N	78.1E	0.0	38.0	04/25/71	03.32.58
KAZ/170/04N	5.5	50.0N	77.7E	0.0	37.6	06/19/71	04.03.58
KAZ/081/04N	5.8	49.7N	78.2E	0.0	38.1	03/22/71	04.32.58
WRS/277/10N	5.1	61.6N	47.1E	13.0	17.3	10/04/71	10.00.02
AUS/005/04N	4.0	47.8N	16.2E	11.0	13.4	01/05/72	04.57.41
WRS/248/07N	4.6	67.7N	33.4E	7.0	11.9	09/04/72	07.00.04
WRS/191/07N	4.6	52.0N	31.0E	33.0	14.1	07/09/72	07.00.08
AUS/169/09N	4.6	48.3N	14.5E	33.0	12.7	06/17/72	0.2.48
GRE/200/13N	4.0	41.6N	23.8E	33.0	20.8	07/18/72	13.45.48
YUG/052/23N	4.0	41.0N	22.3E	33.0	21.0	02/21/72	23.02.55
CAU/079/03N	3.9	42.7N	38.1E	33.0	24.4	03/19/72	03.34.31
BUL/068/22N	3.5	40.8N	22.8E	33.0	21.3	03/08/72	22.04.02
TUR/212/19N	3.6	41.0N	27.0E	33.0	22.2	07/30/72	19.46.24

TABLE III-1
EVENT INFORMATION
(PAGE 2 OF 2)

Event I.D.	m_b	Lat.	Long.	Depth	Δ	Day	Time
AEG/212/01N	4.4	39.9N	24.2E	33.0	22.5	07/30/72	01.30.00
GRE/207/C1N	4.5	38.7N	21.4E	45.0	23.1	07/25/72	01.56.07
CRT/204/05N	4.1	47.0N	36.0E	33.0	20.0	07/22/72	05.10.47
GRE/157/10N	4.2	37.8N	21.4E	69.0	24.0	06/05/72	10.44.59
GRE/153/13N	4.1	39.0N	24.0E	33.0	23.3	06/01/72	13.44.11
WRS/202/15N	3.8	52.0N	54.0E	33.0	24.9	07/21/71	15.49.27
SWR/076/02N	4.1	46.0N	45.4E	33.0	24.9	03/17/71	02.15.46
WRS/295/05N	5.3	51.6N	54.5E	6.0	25.4	10/22/71	05.00.00
GRE/074/15N	4.8	37.2N	24.0E	32.0	25.0	03/15/71	15.23.18
TUR/067/23N	4.7	37.5N	29.7E	21.0	26.2	03/08/71	22.44.47
GRE/109/02N	5.1	39.0N	20.5E	16.0	22.6	04/19/71	02.43.52
TUR/278/18N	4.5	39.0N	29.8E	9.0	24.8	10/05/71	18.53.06
TUR/276/07N	4.7	38.9N	29.9E	23.0	24.9	10/03/71	07.44.27
TUR/161/09N	4.9	39.1N	29.6E	33.0	24.7	06/10/71	09.31.55
TUR/126/04N	4.6	39.0N	29.7E	23.0	24.8	05/06/71	04.24.34
BLS/210/19N	4.5	39.6N	30.4E	33.0	24.4	07/29/71	19.40.10
GRE/187/18N	4.4	37.0N	20.0E	33.0	24.5	07/05/72	18.05.00
WRS/179/12N	3.5	51.0N	47.0E	33.0	22.1	06/27/72	12.20.36
GRE/175/07N	3.4	37.0N	21.0E	33.0	24.7	06/23/72	07.18.14
TUR/175/04N	3.7	41.0N	30.0E	33.0	23.0	06/23/72	04.25.27
TUR/173/05N	4.1	40.2N	30.0E	33.0	23.8	06/21/72	5. 6.17
TUR/167/14N	3.3	38.0N	28.0E	33.0	25.2	05/15/72	14.19.02
GRE/167/00N	4.9	38.3N	22.2E	26.0	23.6	06/15/72	0.33.24
ITA/018/23N	4.1	44.2N	8.2E	25.0	16.7	01/18/72	23.26.12
YUG/067/05N	2.7	43.0N	21.0E	33.0	18.8	03/07/72	05.21.21
YUG/063/21N	4.9	44.7N	18.4E	33.0	16.7	03/03/72	21.26.51
ITA/035/02N	4.8	43.8N	13.3E	25.0	17.1	02/04/72	02.42.19
ITA/039/12N	4.6	43.8N	13.3E	33.0	17.1	02/08/72	12.19.15
ADR/037/01N	4.9	44.0N	13.2E	33.0	16.9	02/06/72	01.34.22
ITA/036/07N	4.7	43.9N	13.3E	33.0	17.0	02/05/72	07.08.13
ITA/036/05N	4.6	43.7N	13.5E	33.0	17.2	02/05/72	05.05.51
ITA/036/03N	4.4	43.2N	13.7E	33.0	17.7	02/05/72	03.49.45
ITA/036/01N	4.8	43.8N	13.3E	33.0	17.1	02/05/72	01.26.23
ITA/035/19N	4.8	43.8N	13.3E	33.0	17.1	02/04/72	19.02.56
ITA/035/17N	4.4	43.8N	13.3E	23.0	17.1	02/04/72	17.19.52
ITA/035/09N	4.4	43.9N	13.2E	23.0	17.0	02/04/72	09.19.32
ITA/035/04N	4.8	43.9N	13.2E	33.0	17.0	02/04/72	04.40.50
SWR/205/11N	3.5	48.0N	28.0E	33.0	16.2	07/24/71	11.11.42
YUG/100/02N	4.6	42.5N	20.1E	21.0	19.2	04/10/71	02.58.06
WES/262/11N	4.5	57.8N	41.1E	33.0	15.6	09/19/71	11.00.00
RUM/251/04N	3.4	45.8N	27.0E	140.0	17.8	09/08/71	04.10.18
YUG/180/01N	4.9	43.0N	20.5E	33.0	18.7	06/28/72	01.43.56
YUG/177/04N	4.4	44.0N	15.8E	33.0	17.1	06/25/72	04.59.19
YUG/176/07N	5.3	43.7N	16.9E	33.0	17.5	06/24/72	07.17.56
ITA/173/15N	4.4	43.8N	13.3E	4.0	17.1	06/21/72	15.06.53
ITA/166/18N	4.9	43.7N	13.4E	14.0	17.2	06/14/72	18.55.53

TABLE III-2
DETECTOR OUTPUT (dB) (1.5-2.5 Hz BAND)
(PAGE 1 OF 4)

Event I.D.	Coh.		Incoh.		Coh.		Incoh.	
	A.D.	D.S.	A.D.	D.S.	A.D.	D.S.	A.D.	D.S.
KUR/142/12N	10.2	8.7	1.6	1.9	12.4	10.7	1.8	2.3
KAZ/070/04N	24.3	25.2	23.0	23.9	47.9	49.9	37.4	40.1
WRS/277/10N	22.7	22.9	20.3	20.8	40.3	41.4	33.6	34.3
URA/082/06N	25.3	25.4	24.8	24.8	63.0	63.2	50.5	51.0
JAP/063/07N	23.1	23.4	17.9	19.0	35.6	36.5	22.9	25.0
EKZ/246/08N	22.9	23.4	18.0	19.3	35.1	37.0	22.9	25.5
EKZ/239/03N	25.2	25.2	23.4	24.0	49.8	51.5	37.8	40.3
EKZ/345/04N	24.4	25.2	23.0	24.1	53.0	54.6	40.9	44.6
EKZ/345/04N	25.1	25.5	23.9	24.5	53.8	55.1	41.6	44.7
SWR/277/08N	24.8	24.8	23.8	23.9	56.5	57.0	45.5	46.1
NZM/241/05N	25.5	25.5	24.8	24.9	62.2	62.9	52.3	52.7
EKZ/363/04N	18.8	19.7	11.0	12.8	23.5	25.1	12.6	14.8
EKZ/229/03N	24.2	24.8	22.1	23.2	44.6	47.5	33.9	37.2
EKZ/188/01N	20.1	21.3	13.6	15.5	27.2	29.3	15.9	18.6
EKZ/041/05N	25.3	25.5	24.3	24.7	54.9	57.7	42.5	45.6
EKZ/364/06N	25.5	25.6	24.7	24.9	58.5	60.3	47.1	48.9
EKZ/349/07N	22.0	22.8	16.5	18.7	31.6	34.2	20.4	23.8
EKZ/333/06N	25.1	25.4	23.4	24.0	48.6	51.2	37.1	40.0
EKZ/294/06N	24.8	25.0	22.4	23.3	46.5	48.5	34.1	37.1
EKZ/159/01N	24.8	25.2	23.0	23.9	45.8	48.7	36.0	39.1
NEV/230/14N	21.8	22.6	17.0	19.4	32.1	34.9	21.8	26.4
CAN/310/22N	25.4	25.4	24.3	24.4	55.0	56.4	44.1	45.2
NZM/270/06N	25.5	25.5	24.9	25.0	62.7	63.2	50.9	51.6
TAD/188/04N	19.3	19.9	12.3	13.4	24.5	25.6	13.9	15.5
IRA/102/19N1	24.7	24.8	23.2	23.5	49.9	50.8	41.2	42.3
KUR/077/03N	20.1	20.3	14.4	15.7	29.5	30.9	18.0	20.2
KAZ/181/04N	23.9	24.3	21.3	22.3	43.9	47.4	33.2	36.2
KM1/073/12N	25.1	25.2	23.7	24.2	51.1	53.4	38.1	40.7
KAZ/356/06N	25.6	25.6	24.9	24.9	56.8	56.9	47.1	47.4
KAZ/282/06N	25.0	25.1	23.0	23.6	46.2	48.4	34.7	37.1
URA/191/16N	25.2	25.3	23.9	24.2	50.5	51.8	40.9	42.4
KAZ/157/04N	25.3	25.4	24.2	24.5	50.7	52.9	40.4	42.7
KAZ/145/04N	23.9	24.4	20.9	21.9	39.4	41.2	28.5	31.0
KAZ/115/03N	25.6	25.6	24.8	24.9	59.2	59.6	47.0	48.0
KAZ/170/04N	25.4	25.4	24.0	24.3	52.3	53.6	39.6	41.6
KAZ/081/04N	25.5	25.5	24.4	24.7	54.1	55.2	42.7	44.6
WRS/295/05N	24.7	24.8	22.7	22.9	51.2	51.1	42.0	43.1
YUG/053/21N	14.8	14.3	7.2	7.3	21.3	21.2	9.6	10.0
ITA/039/12N	12.6	12.0	4.8	4.8	20.2	20.4	9.9	9.6
ITA/036/07N	13.7	14.3	8.1	9.1	20.9	22.3	9.8	11.4
ITA/036/05N	17.6	18.0	9.2	10.1	23.7	24.3	10.6	11.7
ITA/036/03N	13.2	13.5	3.2	3.5	16.4	16.4	5.0	5.3
ITA/036/01N	20.2	20.8	14.2	15.1	31.0	32.1	18.3	19.7
GFE/074/15N	24.6	24.9	21.6	22.5	43.6	44.8	30.6	33.4
YUG/100/02N	19.6	20.7	12.3	14.1	27.4	30.1	18.2	19.7

TABLE III-2
 DETECTOR OUTPUT (dB) (1.5-2.5 Hz BAND)
 (PAGE 2 OF 4)

Event I. D.	Coh.			Incoh.			Coh.			Incoh.		
	A. D.	D. S.	A. D.	D. S.	A. D.	D. S.	A. D.	D. S.	A. D.	D. S.	A. D.	D. S.
TUR/067/23N	13.5	13.8	7.1	7.8	16.3	17.4	7.8	8.7				
GRE/109/02N	21.0	21.7	17.6	18.0	36.7	37.9	25.1	26.5				
AUS/169/09N	20.9	21.2	12.9	13.8	29.5	30.1	15.7	16.9				
ITA/166/18N	17.2	18.0	12.7	13.1	27.0	28.9	20.3	22.1				
GRE/167/00N	23.0	23.2	19.2	19.7	45.1	46.5	33.8	35.1				
ITA/173/15N	10.9	10.4	5.9	5.9	12.3	11.5	6.6	6.5				
YUG/176/07N	19.7	20.1	13.0	13.7	26.6	27.2	15.7	16.7				
YUG/177/04N	21.3	21.3	13.8	15.0	28.0	28.4	16.2	17.9				
YUG/180/01N	13.4	12.8	6.4	6.6	14.9	14.2	9.1	8.9				
GRE/187/18N	18.6	18.5	12.6	13.3	27.7	28.5	16.4	17.7				
WFS/262/11N	22.6	22.9	19.1	20.1	40.0	40.6	33.5	34.9				
TUR/161/09N	20.9	21.2	18.1	18.8	32.3	34.0	26.2	27.5				
TUR/126/04N	17.4	18.0	13.8	14.3	29.1	30.4	21.8	23.1				
BLS/210/19N	19.5	19.8	13.0	14.3	25.3	25.8	15.0	16.7				
TUR/276/07N	16.3	17.0	10.5	11.1	21.7	22.8	12.4	13.1				
TUR/278/18N	18.2	18.8	10.5	11.5	23.7	24.0	11.9	13.2				
GRE/207/01N	22.6	23.0	18.3	18.9	36.4	37.6	25.9	27.3				
AEG/212/01N	16.4	16.8	12.7	13.3	32.9	33.6	20.7	22.0				
WRS/191/07N	22.4	22.3	18.1	19.1	37.5	40.1	37.1	38.6				
WRS/248/07N	23.2	23.8	19.7	21.0	45.9	47.1	34.3	36.7				
ITA/035/02N	16.6	17.2	11.2	11.7	28.7	29.3	16.9	18.2				
ITA/035/04N	12.7	13.0	2.4	2.9	15.6	15.8	2.7	3.2				
ITA/035/09N	13.2	13.3	9.2	9.7	23.5	23.7	12.7	13.6				
ITA/035/19N	13.0	13.0	4.5	4.9	19.7	20.0	7.8	8.3				
ITA/035/17N	19.0	19.6	11.9	12.9	26.6	27.1	14.6	16.0				
ADR/037/01N	21.9	22.4	16.2	17.1	34.4	35.0	22.5	23.8				
GRE/200/13N	19.2	19.5	13.3	14.0	29.0	30.3	17.3	18.7				
ITA/018/23N	17.6	18.4	10.5	12.5	25.3	26.8	12.7	15.4				
YUG/067/05N	17.8	18.2	10.0	10.8	24.0	24.8	11.6	12.6				
YUG/052/23N	18.7	19.2	11.2	12.4	26.7	28.0	13.6	15.2				
CAU/079/03N	12.8	13.1	4.4	4.3	16.4	17.2	5.9	6.1				
SWR/076/02N	13.1	12.6	2.7	2.9	15.0	14.7	2.7	3.0				
WRS/202/15N	11.5	10.9	1.7	2.0	13.2	12.9	2.0	2.3				
SWR/205/11N	13.9	14.3	7.5	8.0	20.4	20.6	10.6	11.3				
TUR/173/05N	11.5	10.7	5.4	5.8	15.6	14.8	7.5	7.9				
TUR/167/14N	16.1	15.6	8.1	8.7	25.2	25.8	13.6	14.9				
GRE/175/07N	13.6	14.5	6.4	8.2	19.9	21.6	9.1	11.9				
TUR/175/04N	14.0	14.7	4.9	6.2	16.5	17.6	5.2	6.5				
WRS/179/12N	14.6	14.5	6.6	7.5	17.4	17.0	7.6	8.2				
RUM/251/04N	19.0	19.5	11.3	12.0	26.0	26.3	14.9	15.8				
GRE/153/13N	17.8	17.9	9.0	9.9	20.5	20.9	10.0	10.9				
GRE/157/10N	22.4	22.7	17.9	18.6	33.7	35.4	22.9	24.2				
CRI/204/05N	24.9	25.1	23.4	23.7	51.2	51.5	40.2	41.1				
TUR/212/19N	16.1	15.8	7.8	8.1	19.7	19.2	8.4	8.6				
AUS/005/04N	15.3	14.9	6.3	6.8	19.5	19.6	7.5	8.0				
BUL/068/22N	16.1	17.5	7.4	9.3	20.2	21.7	8.1	10.4				

TABLE III-2
DETECTOR OUTPUT (dB) (3.0-4.0 Hz BAND)
(PAGE 3 OF 4)

Event I. D.	Coh.		Incoh.		Coh.		Incoh.	
	A. D.	D. S.	A. D.	D. S.	A. D.	D. S.	A. D.	D. S.
KUR/142/12N	8.0	5.8	1.2	2.3	8.4	6.2	1.3	2.1
KAZ/070/04N	24.0	23.8	22.2	22.5	49.6	50.2	38.9	40.1
EK2/345/04N	24.6	24.9	23.6	24.1	59.7	61.2	48.6	50.6
EK1/345/04N	24.1	24.5	23.2	23.7	60.4	62.2	48.5	50.3
SWR/277/08N	24.2	24.0	21.4	21.5	47.0	47.7	38.9	39.9
NZM/241/05N	25.4	25.4	24.1	24.2	57.3	57.7	52.7	52.9
EKZ/363/04N	20.7	20.6	15.0	15.9	27.5	25.8	18.2	19.1
EKZ/229/03N	23.6	23.8	21.5	22.2	42.8	44.1	33.0	34.8
EKZ/188/01N	18.1	18.5	11.7	12.7	23.4	24.0	14.3	15.6
EKZ/041/05N	24.9	25.0	23.3	23.9	51.3	54.5	40.1	43.5
EKZ/246/08N	23.4	23.7	20.1	20.8	38.6	39.5	27.9	29.9
EKZ/239/03N	24.7	25.1	23.5	24.2	51.9	54.9	41.9	44.5
EKZ/364/06N	24.8	24.8	23.3	23.6	51.6	52.8	41.2	43.3
EKZ/349/07N	21.8	22.3	16.1	17.5	33.1	34.7	20.8	23.0
EKZ/333/06N	24.4	24.6	22.6	23.1	47.5	48.9	36.2	38.2
EKZ/294/06N	24.2	24.4	22.1	22.6	45.0	45.7	34.6	36.1
EKZ/159/01N	24.4	24.6	21.8	22.6	40.5	44.3	31.7	34.5
WRS/277/10N	22.4	22.6	21.7	22.1	30.9	41.0	38.0	38.5
NEV/230/14N	5.2	7.4	1.9	3.1	6.1	8.1	2.1	3.4
KAZ/181/04N	24.5	25.0	21.7	23.0	44.2	49.4	33.9	38.0
URA/C82/06N	24.3	24.1	22.8	22.8	53.3	53.8	45.9	46.5
CAN/310/22N	25.4	25.4	24.9	25.0	55.5	55.2	47.7	48.7
NZM/270/06N	25.2	25.2	24.7	24.8	58.1	59.0	51.4	52.2
TAD/188/04N	19.0	20.3	13.7	15.4	24.6	27.1	16.2	18.6
IRA/102/19N1	22.6	23.2	20.8	21.2	39.1	41.5	40.2	42.2
KUR/077/03N	10.4	12.7	8.1	9.5	11.9	14.8	9.5	11.1
KM1/073/12N	23.8	24.3	21.9	23.1	41.7	46.9	32.8	38.3
JAP/063/07N	4.7	4.3	3.6	3.9	7.7	9.7	5.1	5.9
KAZ/356/06N	24.4	24.7	24.3	24.4	47.0	52.2	48.6	50.1
KAZ/145/04N	23.8	24.2	22.4	22.8	40.1	42.4	33.9	35.5
KAZ/115/03N	24.6	24.7	24.8	24.9	55.2	56.9	51.4	52.8
KAZ/170/04N	24.3	24.5	23.2	23.6	45.5	46.7	39.0	40.5
KAZ/081/04N	24.8	24.9	24.5	24.7	52.5	56.3	47.6	49.6
KAZ/282/06N	24.4	24.8	23.3	23.8	46.2	49.8	38.4	41.0
URA/191/16N	24.1	24.3	22.6	22.9	42.8	44.7	38.5	39.1
KAZ/157/04N	23.7	24.4	23.5	24.1	42.2	46.3	39.1	42.0
WRS/295/05N	24.3	24.4	23.3	23.3	47.5	48.6	41.6	42.9
YUG/063/21N	13.0	13.2	4.1	4.4	15.7	16.2	5.2	5.6
ITA/036/07N	13.0	12.7	6.1	6.4	17.0	16.8	7.5	7.9
ITA/036/05N	9.7	9.3	2.6	2.9	12.7	11.7	3.6	4.0
ITA/036/03N	8.1	7.8	1.5	1.9	8.5	8.3	2.2	2.7
ITA/036/01N	17.8	18.2	10.9	11.9	23.5	23.5	12.4	13.7
ITA/039/12N	9.6	9.3	2.8	2.9	12.2	11.8	3.7	3.8
ADR/037/01N	20.8	21.4	14.4	16.0	28.8	31.1	17.7	20.3
WES/262/11N	23.4	23.1	21.6	21.5	48.5	48.6	43.8	43.5

TABLE III-2
DETECTOR OUTPUT (dB) (3.0-4.0 Hz BAND)
(PAGE 4 OF 4)

Event I. D.	Coh.		Incoh.		Coh.		Incoh.	
	A. D.	D.S.	A. D.	D.S.	A. D.	D.S.	A. D.	D.S.
TUR/161/09N	4.9	7.7	3.9	4.4	6.2	8.3	10.8	11.1
TUR/126/04N	5.3	7.1	9.3	9.4	6.2	8.3	4.2	4.4
BLS/210/19N	4.6	6.4	4.0	4.2	3.7	6.0	4.2	4.4
ITA/035/19N	16.2	15.5	7.6	7.9	18.3	17.6	8.0	8.6
ITA/035/17N	15.6	14.7	6.2	6.8	18.8	18.1	7.8	8.6
ITA/035/09N	11.6	11.4	4.6	4.1	15.4	14.7	5.4	4.8
ITA/035/04N	7.8	7.3	1.5	1.5	10.1	9.5	1.6	1.6
ITA/035/02N	15.9	15.9	11.8	12.5	20.6	20.6	14.2	15.0
GRE/074/15N	18.7	20.9	17.0	18.1	20.7	25.5	20.2	21.9
YUG/100/02N	13.4	15.4	12.4	13.3	20.1	20.7	17.7	18.0
TUR/067/23N	4.4	4.9	1.9	2.6	5.1	5.7	2.0	2.7
GRE/109/02N	22.2	22.2	18.0	18.9	36.1	37.3	24.7	26.7
ITA/166/18N	15.9	16.1	9.0	9.9	22.6	23.3	11.5	13.0
GRE/167/00N	22.1	22.4	16.2	17.0	32.3	32.9	20.2	21.6
YUG/180/01N	8.2	6.7	1.8	2.2	9.1	7.2	1.6	2.2
GRE/187/18N	15.4	15.8	9.7	10.6	21.7	22.0	11.7	13.2
YUG/177/04N	14.1	12.2	5.4	5.9	15.6	12.3	5.5	5.8
YUG/176/07N	13.9	13.7	5.7	7.2	15.5	16.0	6.5	8.4
AUS/169/09N	15.4	15.6	7.3	7.9	18.5	19.1	8.1	9.0
ITA/173/15N	9.1	8.9	2.4	2.8	10.6	9.5	3.0	2.9
TUR/278/18N	13.1	12.9	3.8	4.2	15.2	14.9	4.5	4.9
TUR/276/07N	9.9	9.5	2.6	2.6	10.8	10.2	2.6	2.6
GRE/207/01N	17.5	18.1	12.4	12.9	27.0	27.8	17.4	18.1
WRS/191/07N	24.0	23.9	21.1	21.2	42.6	43.3	45.5	46.1
WRS/248/07N	22.1	22.3	20.4	20.7	45.5	45.9	33.5	34.6
AEG/212/01N	13.7	11.9	7.4	6.8	21.3	18.9	11.0	10.7
GRE/200/13N	15.8	16.4	9.6	10.5	20.5	21.7	11.7	12.8
ITA/018/23N	11.8	13.1	5.3	6.4	16.5	17.2	6.7	7.7
YUG/067/05N	12.4	11.0	5.1	5.4	13.5	11.0	5.8	5.9
YUG/052/23N	11.3	9.1	3.0	3.5	11.7	9.1	3.3	4.3
BUL/068/22N	9.8	6.8	3.2	4.1	12.3	12.4	4.2	6.7
CAU/079/03N	5.9	5.0	3.9	4.6	5.7	3.2	5.1	4.2
RUM/251/04N	18.4	18.3	12.6	12.5	25.9	25.7	16.2	16.1
AUS/005/04N	14.6	14.1	7.7	7.8	20.6	20.2	10.8	11.1
SWR/076/02N	15.8	15.3	7.6	8.1	19.4	18.8	8.7	9.2
WRS/202/15N	8.4	8.3	1.9	3.7	9.7	11.2	2.3	4.9
SWR/205/11N	14.3	13.8	5.1	5.0	20.4	19.8	9.4	9.4
TUR/173/05N	13.3	10.9	5.2	4.5	14.8	11.9	5.8	5.0
TUR/167/14N	12.5	11.9	5.8	5.7	16.7	16.1	7.2	7.6
WRS/179/12N	10.1	8.9	2.5	2.8	12.6	11.1	3.3	3.8
TUR/175/04N	6.7	4.4	1.3	1.7	8.1	5.0	1.5	1.9
GRE/175/07N	9.7	9.2	1.7	1.8	10.3	9.5	1.8	1.8
GRE/153/13N	10.4	9.8	2.8	3.4	12.7	11.4	3.0	3.6
GRE/157/10N	16.5	16.7	9.5	10.0	20.5	20.8	12.8	13.3
CRI/204/05N	24.1	24.2	22.2	22.4	49.2	49.9	36.9	37.7
TUR/212/19N	10.0	8.8	1.3	1.4	11.3	10.0	1.3	1.3

TABLE III-3
NOISE SAMPLES

Year/ Day	(Month/ Day/ Year)	Start Time (Hour:Minute:Second)	Length (Seconds)
71/060	(03/01/71)	06:58:05. 3	320
71/067	(03/08/71)	22:45:40. 9	320
71/074	(03/15/71)	15:22:55. 7	320
71/074	(03/15/71)	14:51:31. 5	320
71/099	(04/09/71)	15:13:17. 9	320
71/099	(04/09/71)	04:01:31. 4	320
71/105	(04/15/71)	18:56:39. 3	320
71/214	(08/02/71)	03:02:20. 5	320
71/217	(08/05/71)	01:10:56. 8	320
71/123	(05/03/71)	00:37:14. 5	320

SECTION IV

RESULTS AND DISCUSSIONS

A. INTRODUCTION

This section presents the results of the computation and processing of the events and noise samples. Subsection B illustrates the computation of beams, and the associated averages (or envelopes) and the detector output. Subsection C discusses the false alarm probability measurements. Following in Subsection D is the discussion of detection probability measurements. The operating characteristics of the detectors are presented and compared in the last subsection.

B. ILLUSTRATION OF COMPUTATION

Figure IV-1 shows coherent and incoherent adjusted-delay and diversity-stack beams (AB), and the associated short-term averages (STA) and long-term averages (LTA) for a signal of a presumed explosion from Kazakh. In this figure, all array beams are plotted with the same scale factor but the associated averages are enlarged by a factor $1.2 \times (AB)_{\max} / STA_{\max}$ in each case. The shape of the STA approximately reflects the envelope and duration of the P-wave although it is delayed by the 1.5 second integration time. An adjusted-delay beamformer is used in the NORSAR on-line system, but the diversity-stack beamformer yields the better signal-to-noise processing gain, and hence, potentially provides an improvement in detectability. Figure IV-2 illustrates the same computations for a noise sample from day 214 of 1971. Because the associated STA and LTA averages of the noise are also multiplied by the factor given above, STA and LTA appear slightly larger than AB.

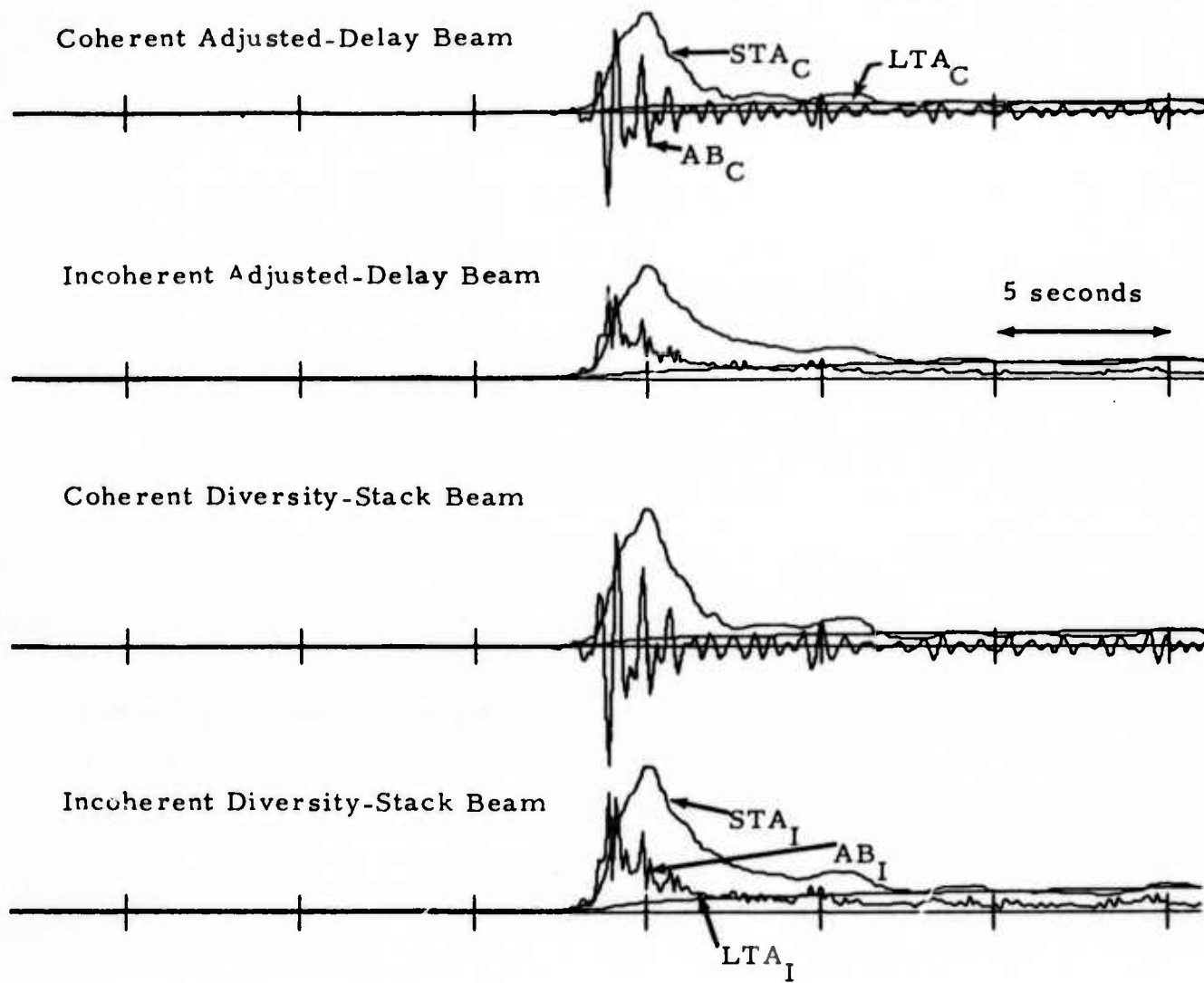


FIGURE IV-1
AN ILLUSTRATION OF ARRAY BEAMS, STAS AND LTAS
(KAZ/282/06N, 1.5-2.5 Hz)

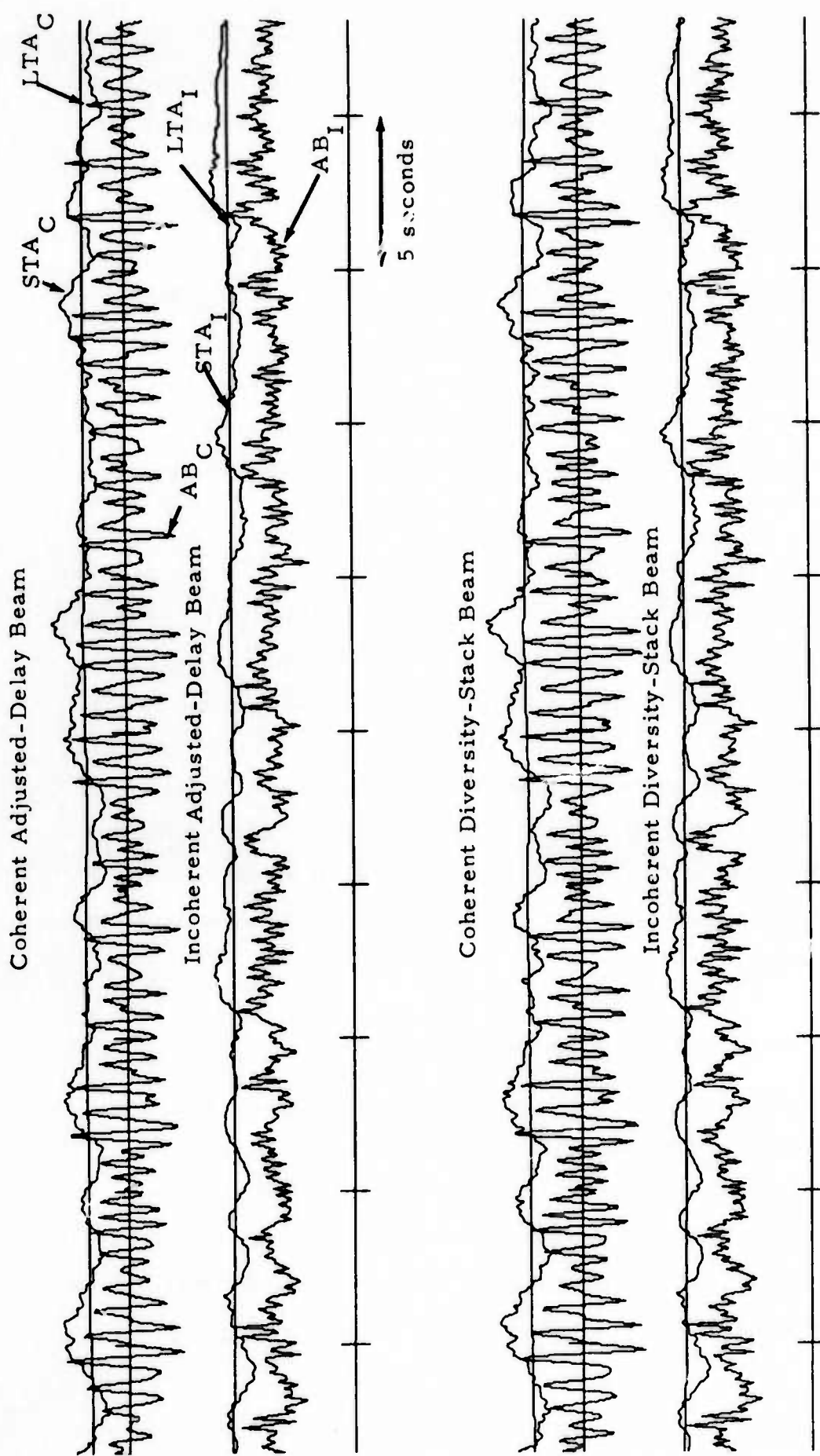


FIGURE IV-2
AN ILLUSTRATION OF ARRAY BEAMS, STA_S, STA_I, LTAS
(DAY 214 OF 1971 NOISE, 1.5-2.5 Hz)

Figure IV-3 shows the beams and the associated envelopes and long-term averages for the same event shown in Figure IV-1, but where the Hilbert transform is used for the envelope formation. All the traces, beams and envelopes, have the same plot scale factor in this figure. This method produces an obviously more accurate representation of the envelope than the STA technique and greatly increases the detectability of P-wave amplitudes as shown in the figure. Figure IV-4 repeats the same illustration for a noise sample from day 214 of 1971. Note that due to the absence of noise cancellation involved in incoherent array beamforming, the incoherent envelopes have the higher amplitudes; but that the variability of the STA output is less for the incoherent beam.

Figures IV-5 and IV-6 illustrate the detector output for an event from Kazakh and a noise sample from day 214 of 1971, respectively. In these figures, the output is the running signal-to-noise ratio, $\text{SNR}(t)$ of equation (II-13). Since each trace has a different plot scale-factor, it does not reflect the performance of detectors. For Figure IV-5, the peak values, $(\text{STA}/\text{LTA})_{\text{max}}$ are shown in Table III-2. Figures IV-7 and IV-8 show the same illustrations for the event in Figure IV-5 and the noise in Figure IV-6, but using a Hilbert transformation. The higher variabilities of detector output by use of Hilbert transformation reflect more degrees of freedom for the analytic envelopes than for the STA envelopes.

C. THE MEASURED FALSE ALARM PROBABILITY

As an illustration, Figure IV-9 shows a histogram of detector output from an incoherent noise beam. This curve was normalized to one at maximum density. The measured mean value and standard deviation are -0.053 dB and 0.691 dB, respectively. In the lower part of the figure is shown the number of counts within a certain output range. For example, there are 9 counts (out of a total of 2900) in the range from 2.0 to 2.2 dB.

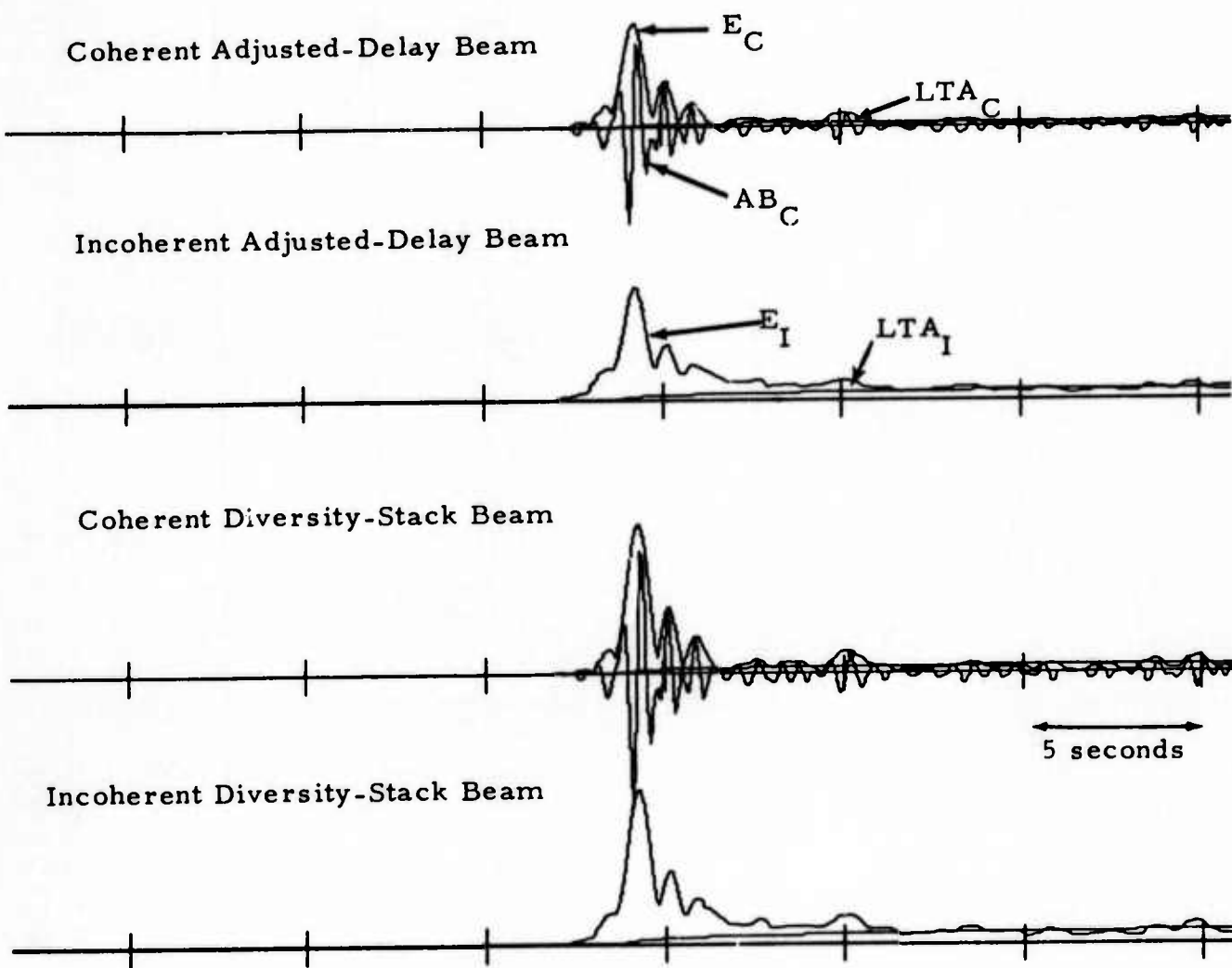
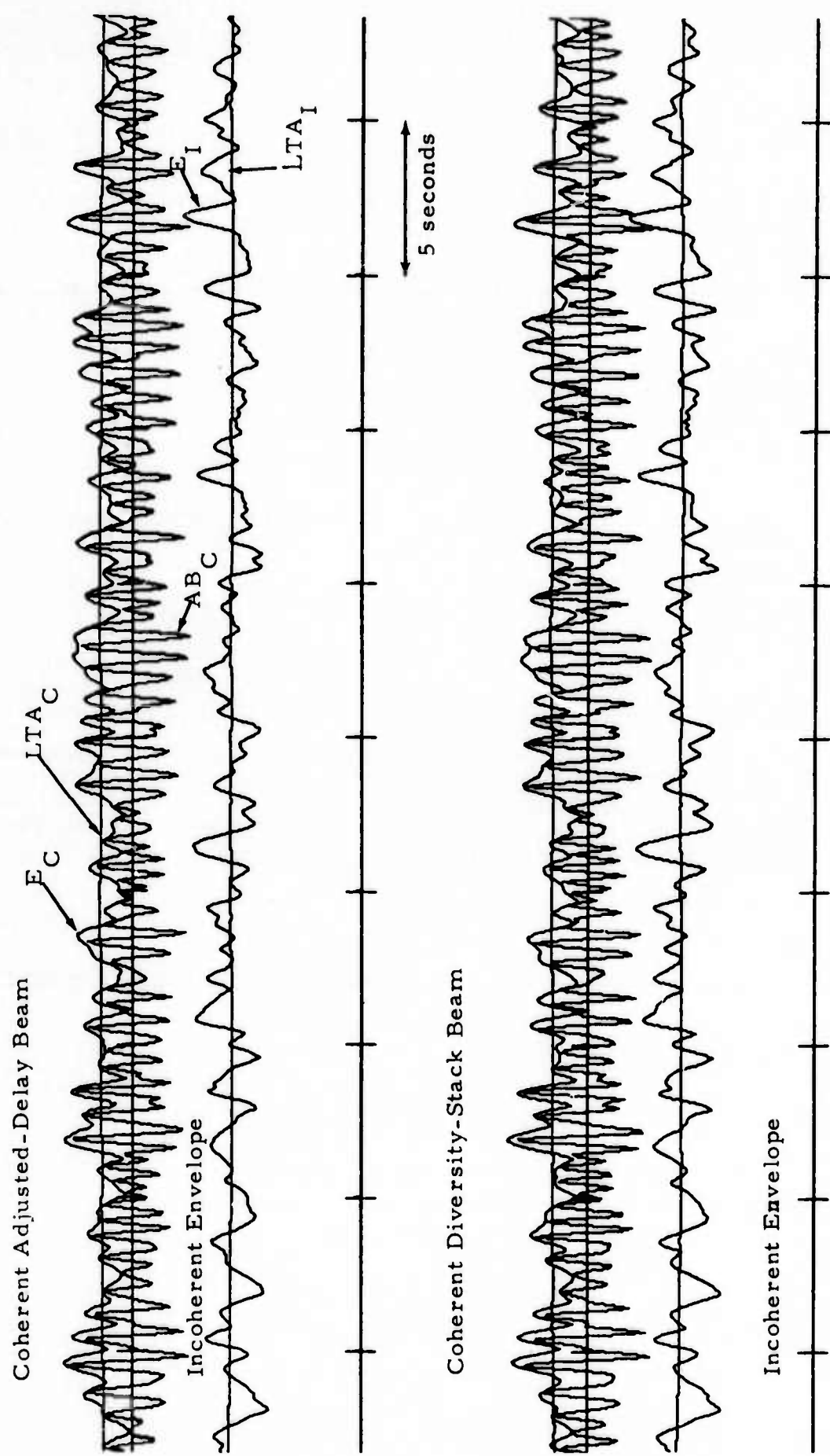


FIGURE IV-3
AN ILLUSTRATION OF ARRAY BEAMS,
ENVELOPES AND LTAS USING HILBERT TRANSFORM
(KAZ/282/06N, 1.5-2.5 Hz)



IV-6

FIGURE IV-4
AN ILLUSTRATION OF ARRAY BEAMS, ENVELOPES, AND LTAS USING HILBERT TRANSFORM
(DAY 214 OF 1971 NOISE, 1.5-2.5 Hz)

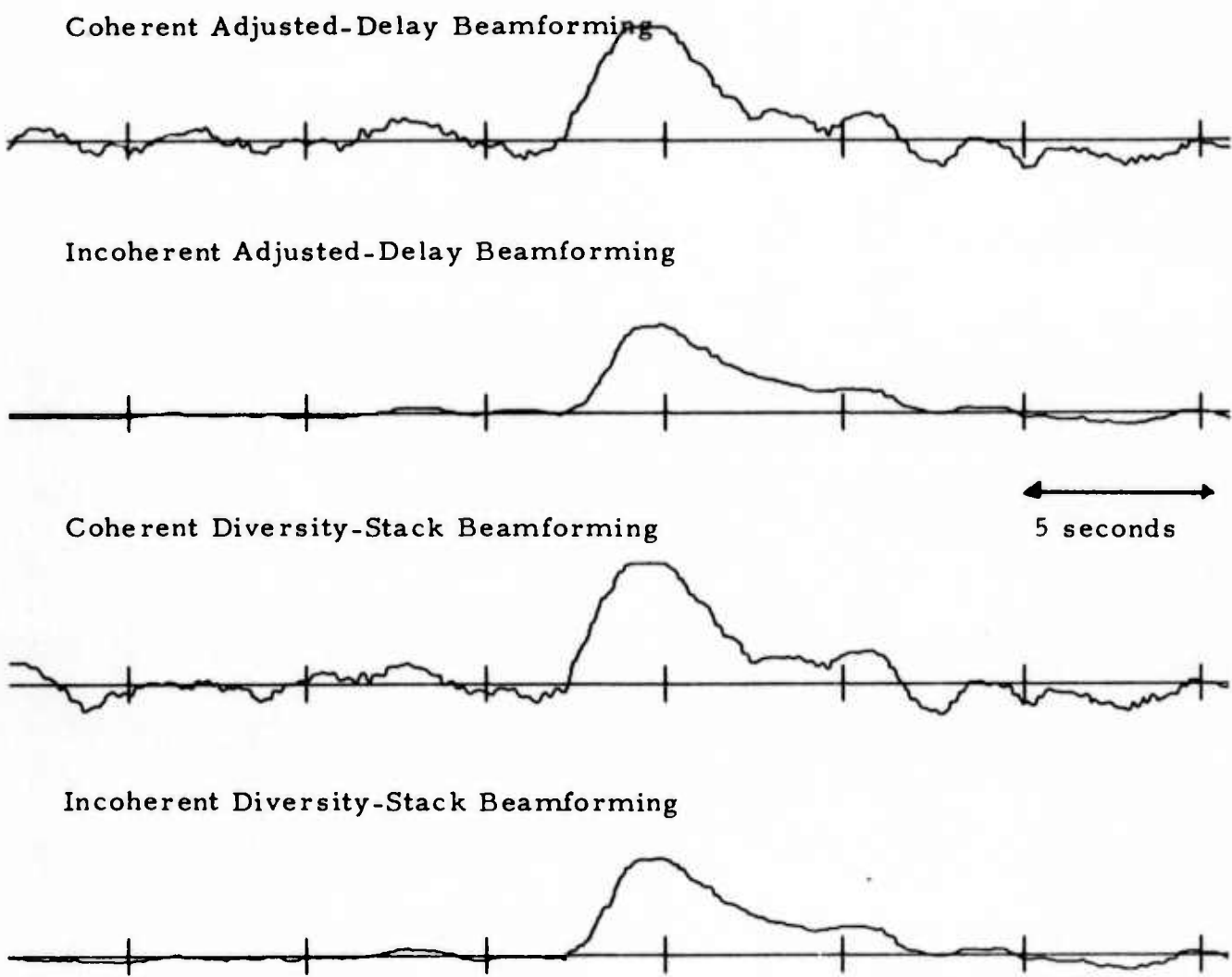


FIGURE IV-5
AN ILLUSTRATION OF DETECTOR OUTPUT, SNR
(KAZ /282/06N, 1.5-2.5 Hz)

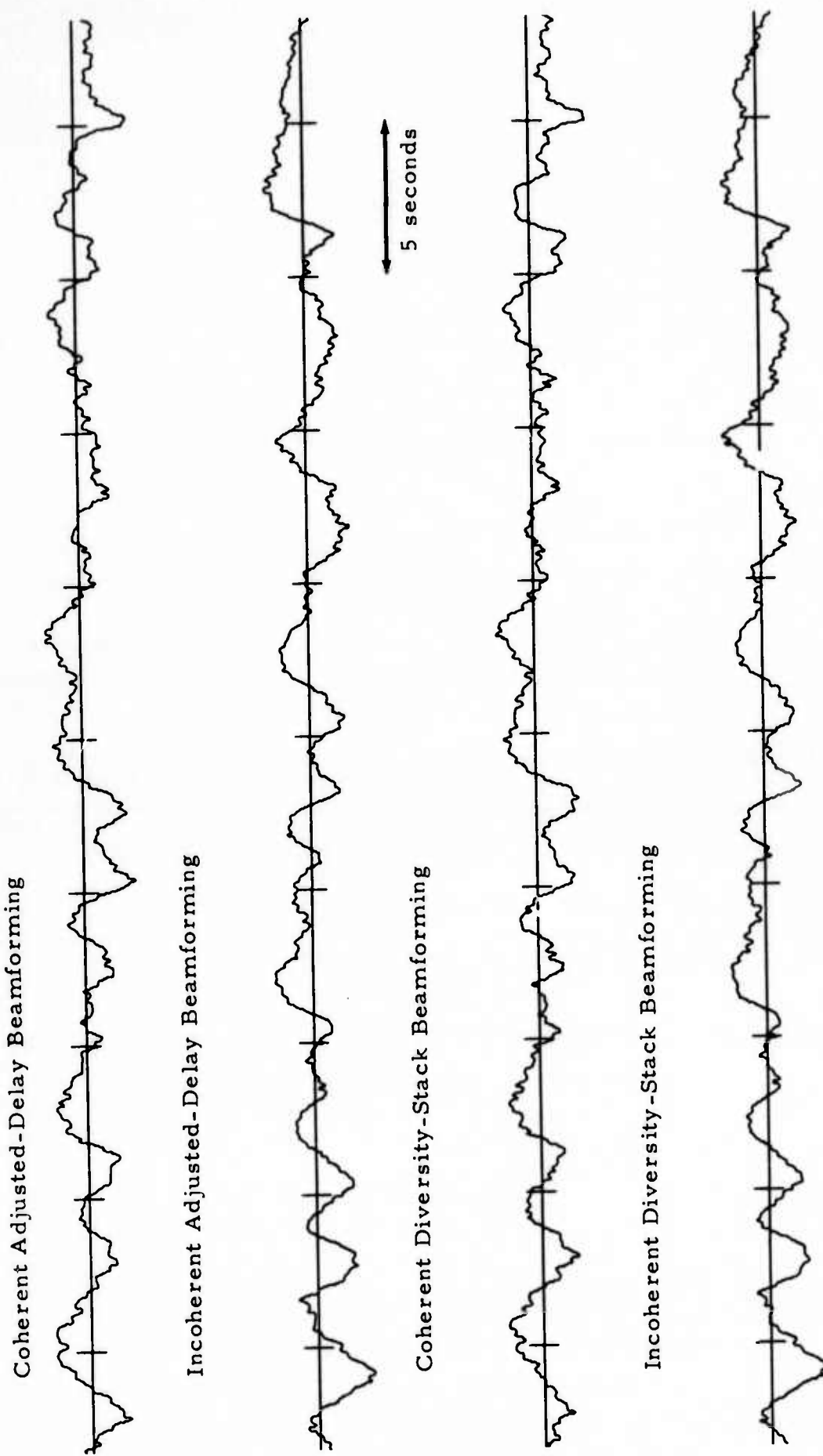
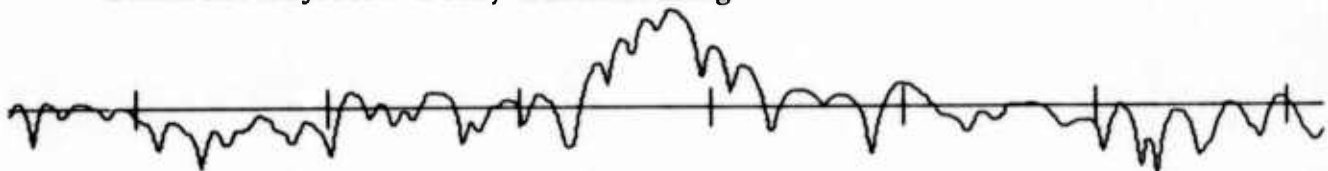
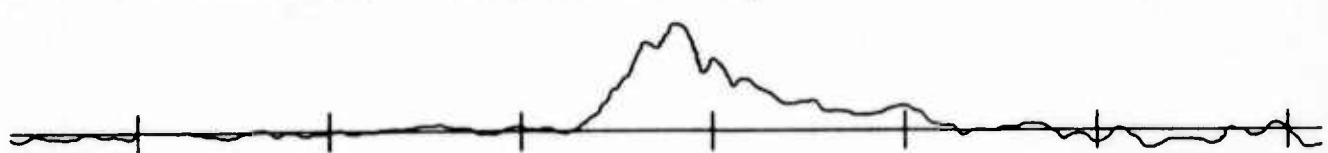


FIGURE IV-6
AN ILLUSTRATION OF DETECTOR OUTPUT, SNR
(DAY 214 1971 NOISE, 1.5-2.5 Hz)

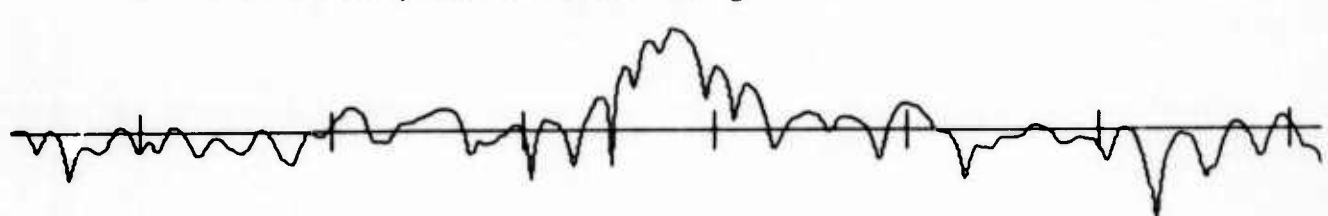
Coherent Adjusted-Delay Beamforming



Incoherent Adjusted-Delay Beamforming



Coherent Diversity-Stack Beamforming



5 seconds

Incoherent Diversity-Stack Beamforming

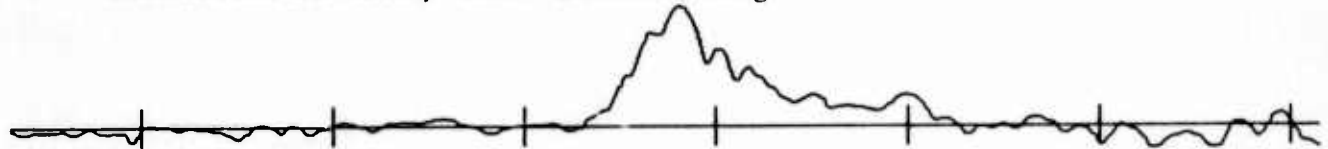
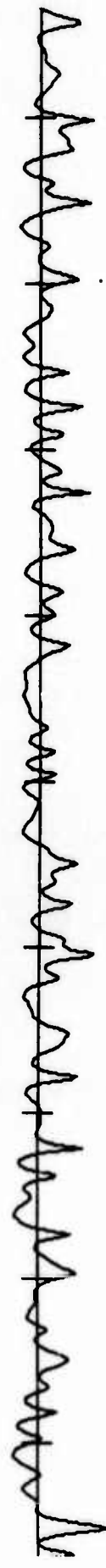


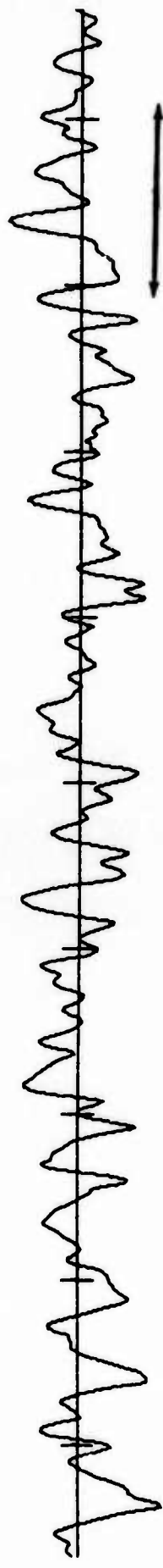
FIGURE IV-7

AN ILLUSTRATION OF DETECTOR OUTPUT USING HILBERT TRANSFORM
(KAZ/282/06N, 1.5-2.5 Hz)

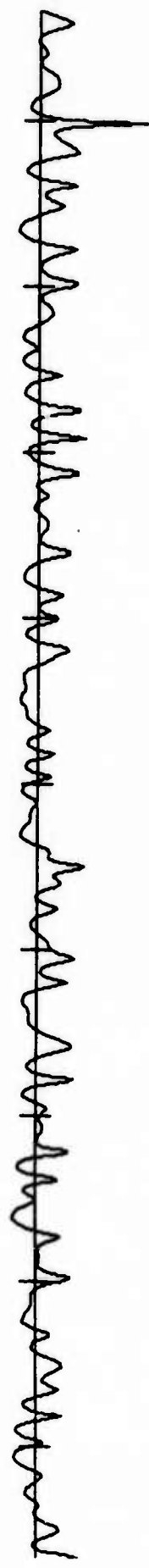
Coherent Adjusted Delay Beamforming



Incoherent Adjusted Delay Beamforming



Coherent Diversity-Stack Beamforming



Incoherent Diversity-Stack Beamforming

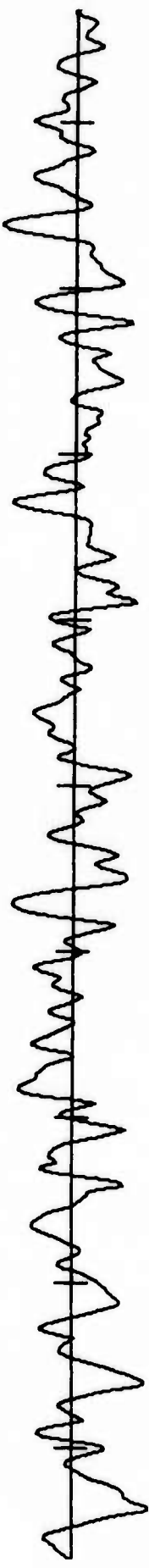


FIGURE IV-8

AN ILLUSTRATION OF DETECTOR OUTPUT USING HILBERT TRANSFORM
(DAY 214 1971 NOISE, 1.5-2.5 Hz)

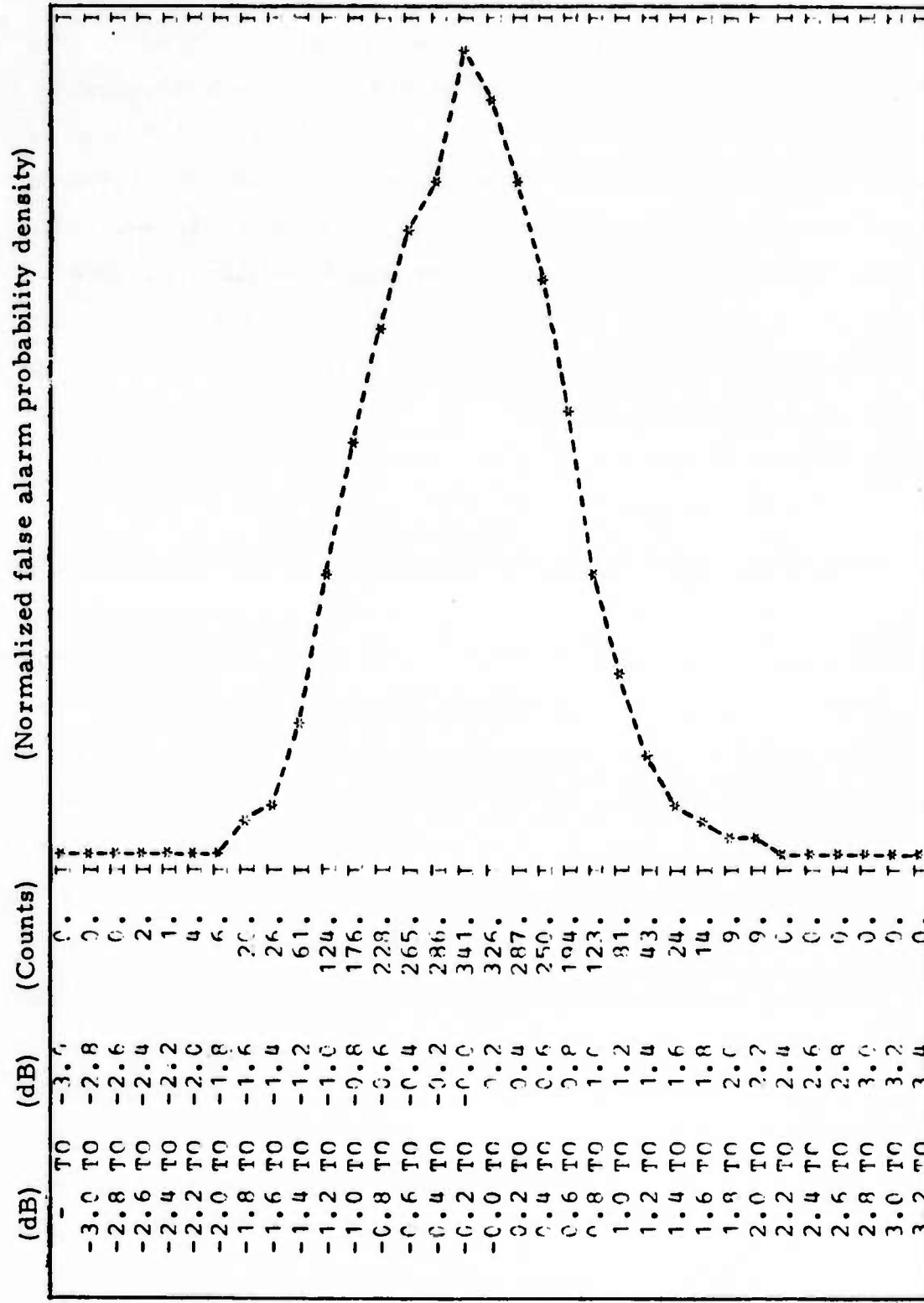


FIGURE IV-9
FALSE ALARM HISTOGRAM FOR AN INCOHERENT DETECTOR
(DAY 214 OF 1971 NOISE, 1.5-2.5 Hz)

Figures IV-10 and IV-11 show the false alarm probability distributions for the coherent and incoherent detectors computed from ten noise samples for the adjusted-delay beams in the 1.5-2.5 Hz and 3.0-4.0 Hz passbands, respectively. The standard deviations of the probability for a given detector output level among the ten noise samples are indicated for several discrete points. The arrows indicate that the standard deviation is greater than the mean value for that specific level, which means that the experimental false alarm probabilities can possibly be zero. Figures IV-12 and IV-13 show the false alarm probability distributions for the diversity-stack beams in the 1.5-2.5 Hz and 3.0-4.0 Hz passbands, respectively. They were computed from the same ten noise samples.

The noise beams were formed at infinite velocity (vertical beams) since, as will be discussed later, the noise is essentially uncorrelated between subarrays at NORSAR (Barnard and Whitelaw, 1972). For the diversity-stack beams, the probability curves closely follow a Gaussian distribution but, the tails of the adjusted-delay curves behaved erratically and deviated from a Gaussian distribution in both passbands. This is partially due to the limited data base. The diversity-stack curves are more well-behaved because the weighting coefficient of each channel was proportional to the reciprocal of the noise power and thus tended to suppress the erratic channels.

The discussion of false alarm rate measurement will be based on the diversity-stack beams because it is more uniformly distributed and it is believed that the results will be more reliable. Comparing the results between Figures IV-12 and IV-13, the false alarm probability in the 1.5-2.5 Hz passband is higher than that in the 3.0-4.0 Hz passband for the coherent detector while the opposite is true for the incoherent detector. For example, having the false alarm probability at the 10^{-3} level, the decision threshold is 7.5 dB in the 1.5-2.5 Hz passband and 7.0 dB in the 3.0-4.0 Hz passband for the coherent detector. This difference increases at lower probability levels. For an incoherent

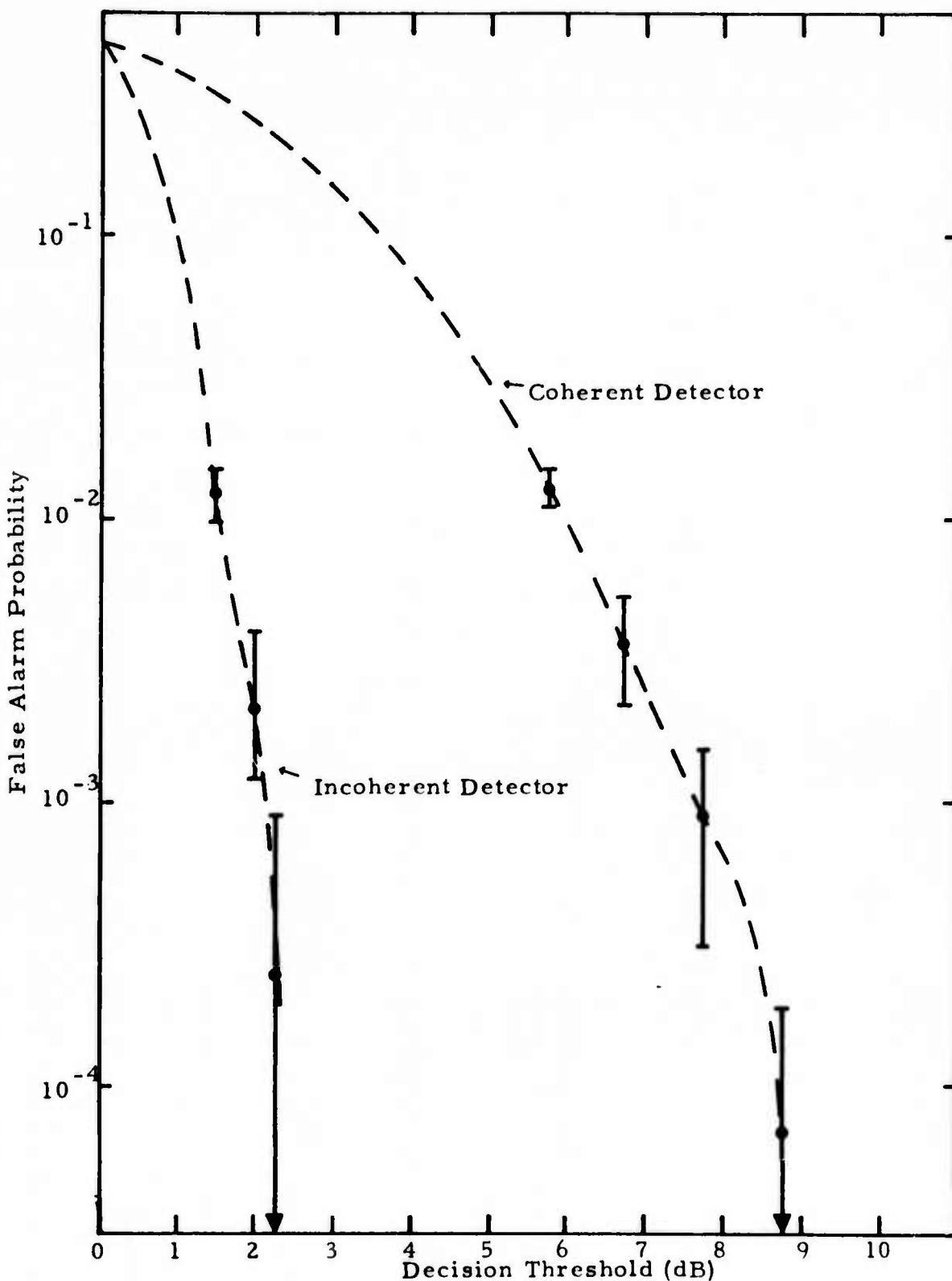


FIGURE IV-10

FALSE ALARM PROBABILITY FOR ADJUSTED-DELAY BEAM
IN THE 1.5-2.5 Hz PASSBAND (FROM TEN NOISE SAMPLES)

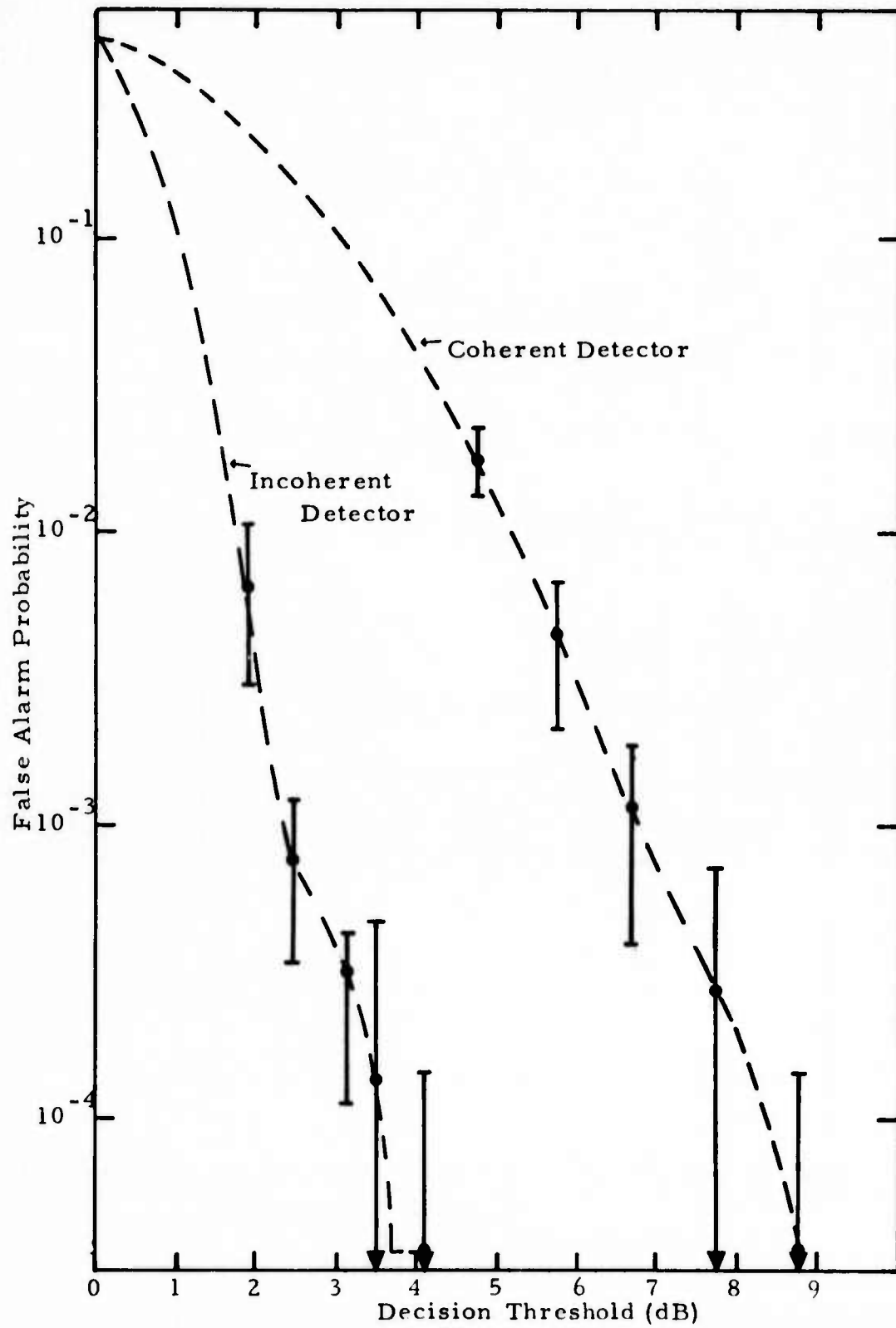


FIGURE IV-11

FALSE ALARM PROBABILITY FOR ADJUSTED-DELAY BEAM
IN THE 3.0-4.0 Hz PASSBAND (FROM TEN NOISE SAMPLES)

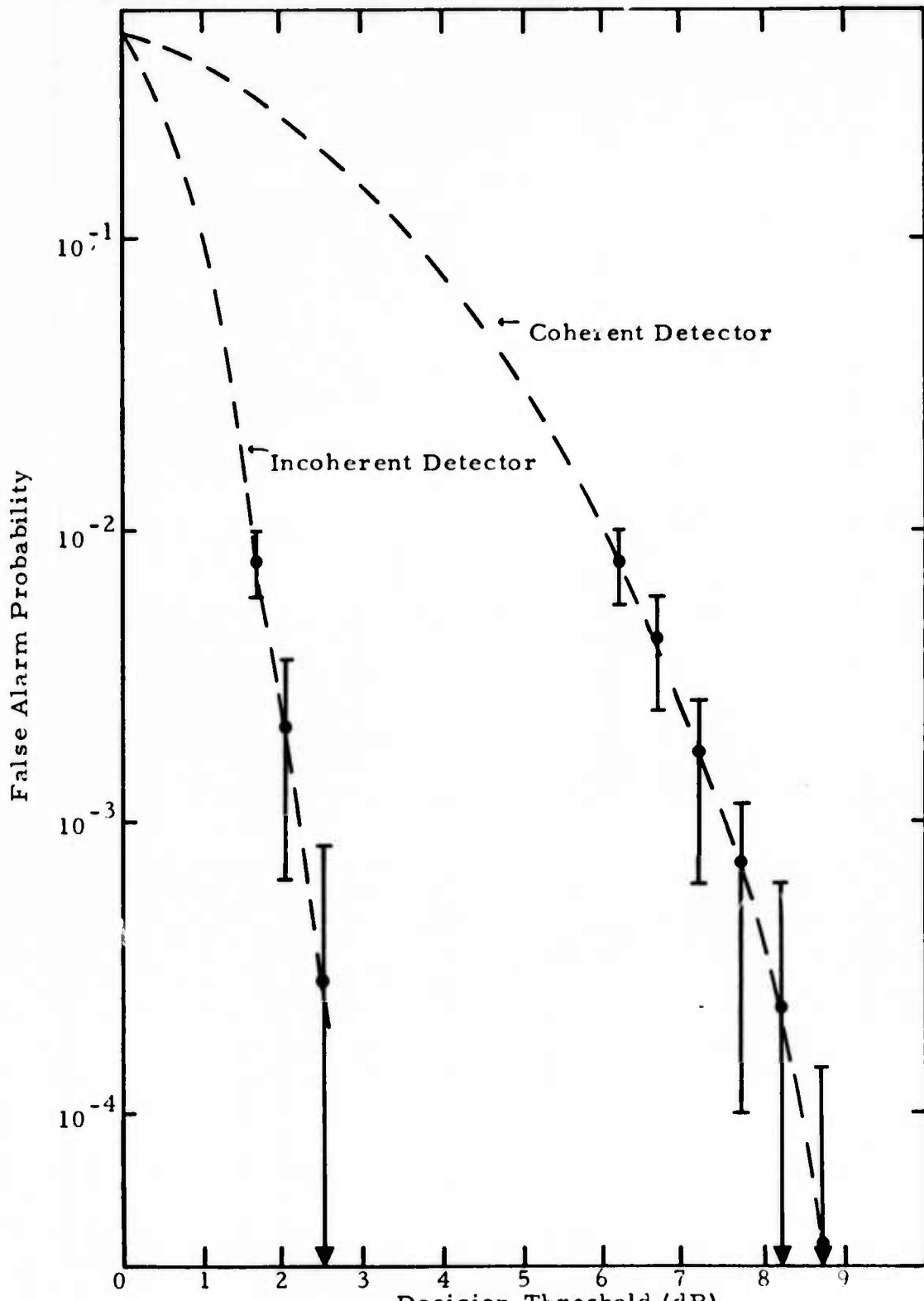


FIGURE IV-12

FALSE ALARM PROBABILITY FOR DIVERSITY-STACK BEAM
IN THE 1.5-2.5 Hz PASSBAND (FROM TEN NOISE SAMPLES)

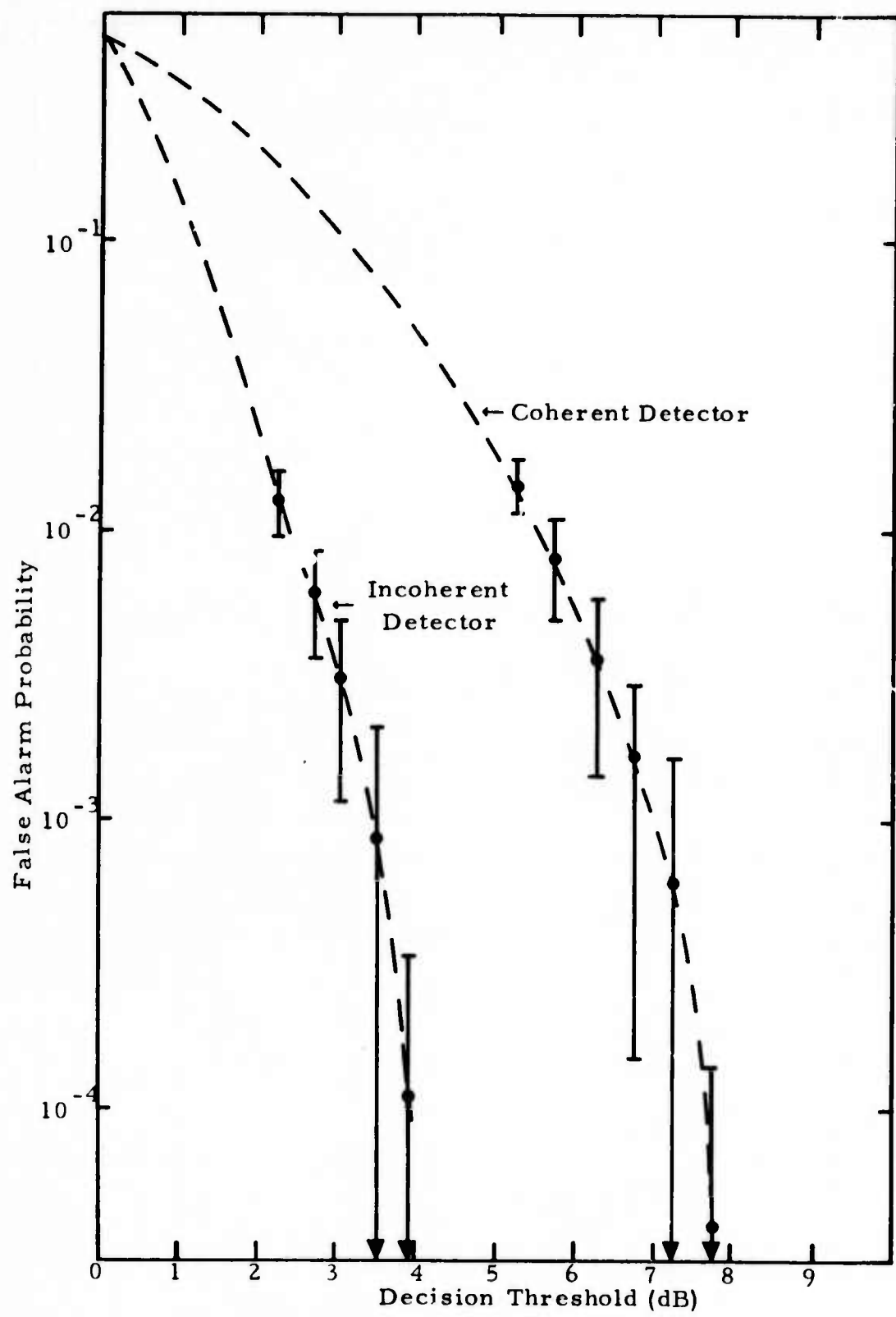


FIGURE IV-13

FALSE ALARM PROBABILITY FOR DIVERSITY-STACK BEAMS
IN THE 3.0-4.0 Hz PASSBAND (FROM TEN NOISE SAMPLES)

detector having the same 10^{-3} level, the decision threshold is 2.3 dB in the 1.5-2.5 Hz passband and 3.5 dB in the 3.0-4.0 Hz passband. Therefore, the false alarm rate is much higher in the higher frequency passband for an incoherent detector.

The explanation of this result is given below. Previous short-period analysis indicated that the noise was almost completely uncorrelated among subarrays because of the large distances involved (IBM, 1970). The multiple coherence between the reference sensor of subarray 1 and the reference sensors of subarrays 2, 3, 4, 6, and 8 for one noise sample was about 0.14 in the 1.5-2.5 Hz passband and 0.1 in the 3.0-4.0 Hz passband (Barnard and Whitelaw, 1972, Figure II-9). This could account for the higher false alarm probability in the 1.5-2.5 Hz passband than in the 3.0-4.0 Hz passband for the coherent detector. However, the noise coherence was higher in the 3.0-4.0 Hz passband than in the 1.5-2.5 Hz passband within a subarray at NORSAR (Barnard and Whitelaw, 1972, Figure II-8; Capon, 1972, Figure IV-15). This could account for the greater false alarm rate in the 3.0-4.0 Hz passband than in the 1.5-2.5 Hz passband with the incoherent beam because it is essentially the average of the subarray beams.

Lacoss (1972) using NORSAR data theoretically estimated the false alarm probability for the 10.5 dB level at 1.1×10^{-5} for the coherent detector. From Figures IV-12 and IV-13, the decision threshold would be slightly lower than that for the coherent detector. But, for the incoherent detector, the threshold must be higher than the 3.0 dB level in the 1.5-2.5 Hz passband and the 4.5 dB level in the 3.0-4.0 Hz passband. Table IV-1 shows the statistical parameters derived from the observed probability curves shown in Figures IV-10 through IV-13. In using these parameters to estimate the false alarm probability it must be noted that the estimated probability could be higher than actually shown in Figures IV-10 through IV-13 in the tail because the experimental curves go to zero there. For example, with the diversity-stack coherent

TABLE IV-1
STATISTICAL PARAMETERS DERIVED FROM
FIGURES IV-10 THROUGH IV-13

Parameters	Beams	Coherent Detector (dB)			Incoherent Detector (dB)
		1.5-2.5 Hz	3.0-4.0 Hz	1.5-2.5 Hz	3.0-4.0 Hz
Mean	Adjusted-delay	-0.48	-0.36	-0.04	-0.02
	Diversity-stack	-0.48	-0.38	-0.04	-0.04
Standard Deviation	Adjusted-delay	3.02	2.68	0.70	0.70
	Diversity-stack	2.99	2.70	0.72	0.94

detector, in order to achieve a false alarm rate less than 3.17×10^{-5} , we must have $(S + 0.38) / 2.70 = 4.0$ or $S = 10.42$ dB. This is higher than what Figure IV-13 indicates.

D. DETECTION PERFORMANCE

1. Comparison of Outputs From Coherent and Incoherent Detectors

One of the objectives of this study was to compare the performance of coherent and incoherent detectors on signals from close events where conventional coherent beamforming is occasionally ineffective. This problem is compounded by signals with particularly strong high-frequency energy such as from close events where attenuation of that energy is not as great. The analysis of the 91 events listed in Table III-1 was oriented toward a study of these effects.

Figures IV-14 through IV-21 are the plots of the coherent detector output (in dB) versus the incoherent detector output. The first four figures illustrate the results in the 1.5-2.5 Hz passband using adjusted-delay and diversity-stack beams for the $(STA/LTA)_{max}$ mode and the $(STA)_{max} / \overline{LTA}$ mode, respectively. The next four figures repeat the same illustrations for the 3.0-4.0 Hz passband. The presumed explosions and the earthquakes are identified by different symbols as indicated on the figures.

The coherent detector performed better than the incoherent detector in the lower frequency band than in the higher frequency band. Figures for the 3.0-4.0 Hz passband seem to suggest that the incoherent detector tends to perform better, particularly for the lower magnitude events. Hence, for detecting the small events, the incoherent detector operating in the higher frequency band would be valuable. However, for better comparison of the detector's performance, it is necessary to compare the operating characteristics of the detectors involved.

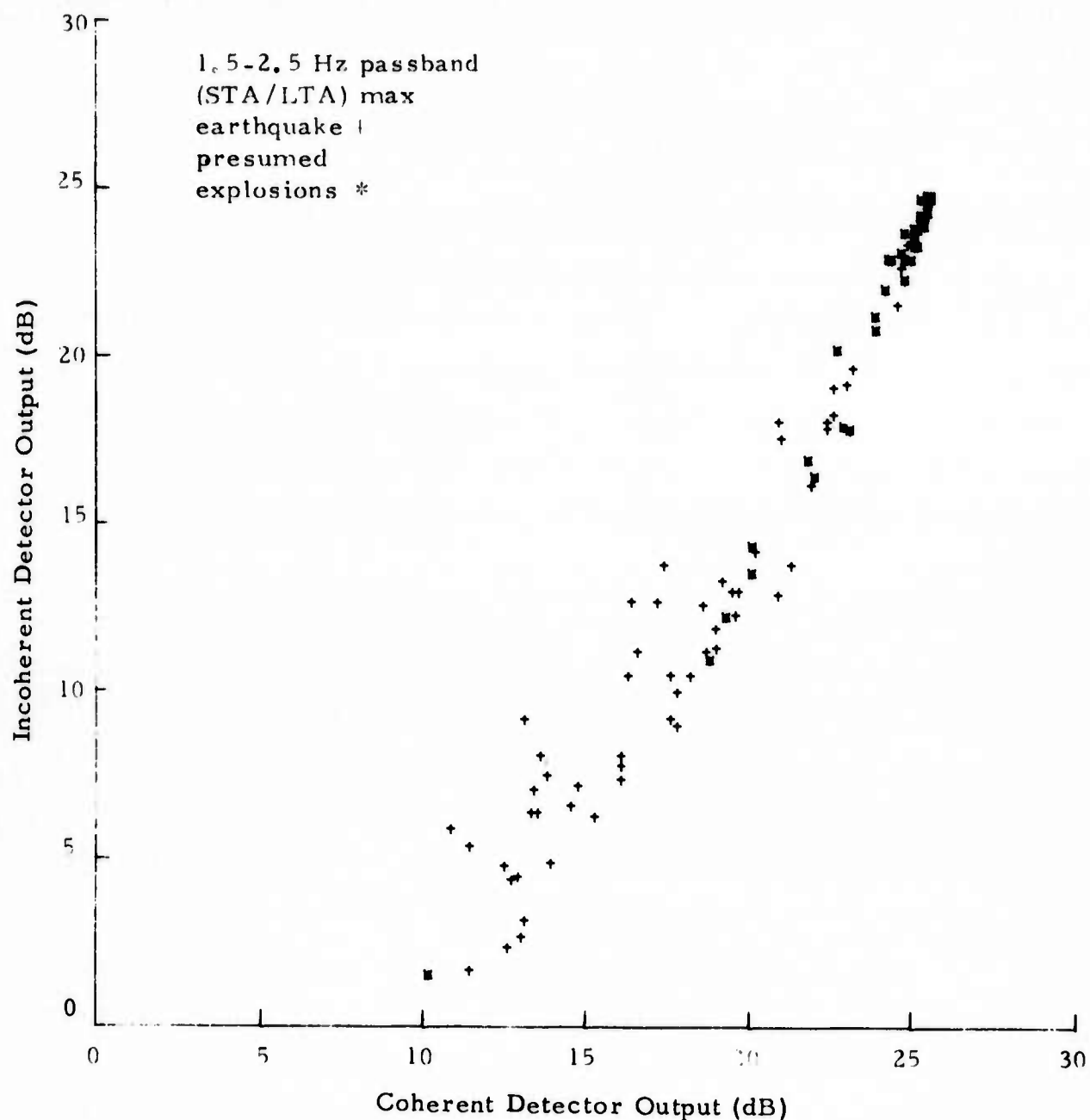


FIGURE IV-14
COHERENT ADJUSTED-DELAY DETECTOR OUTPUT VERSUS
INCOHERENT DETECTOR OUTPUT
((STA/LTA)_{max} IN THE 1.5-2.5 Hz PASSBAND)

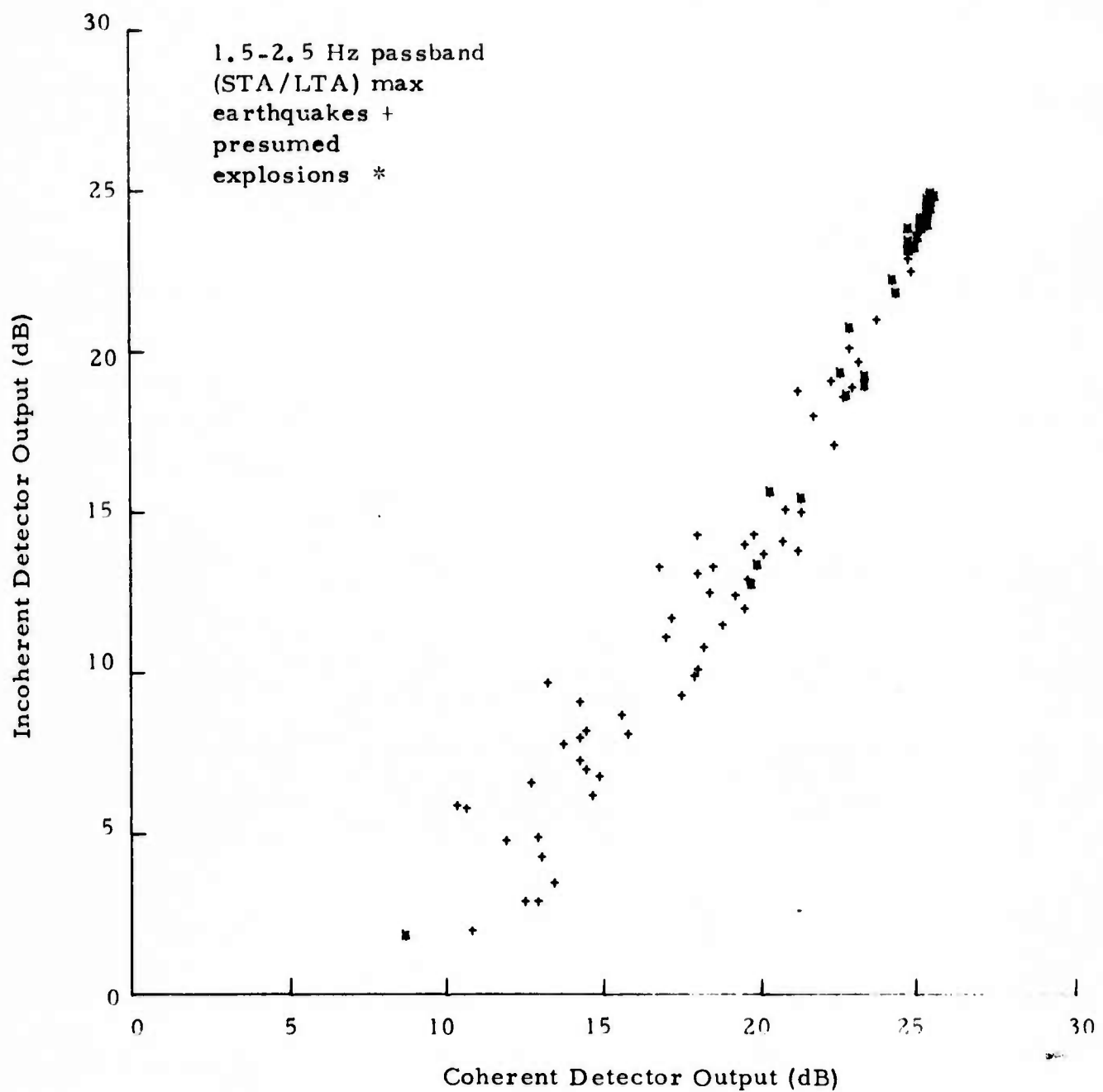


FIGURE IV-15
COHERENT DIVERSITY-STACK DETECTOR OUTPUT VERSUS
INCOHERENT DETECTOR OUTPUT
 $(\text{STA/LTA})_{\max}$ IN THE 1.5-2.5 Hz PASSBAND)

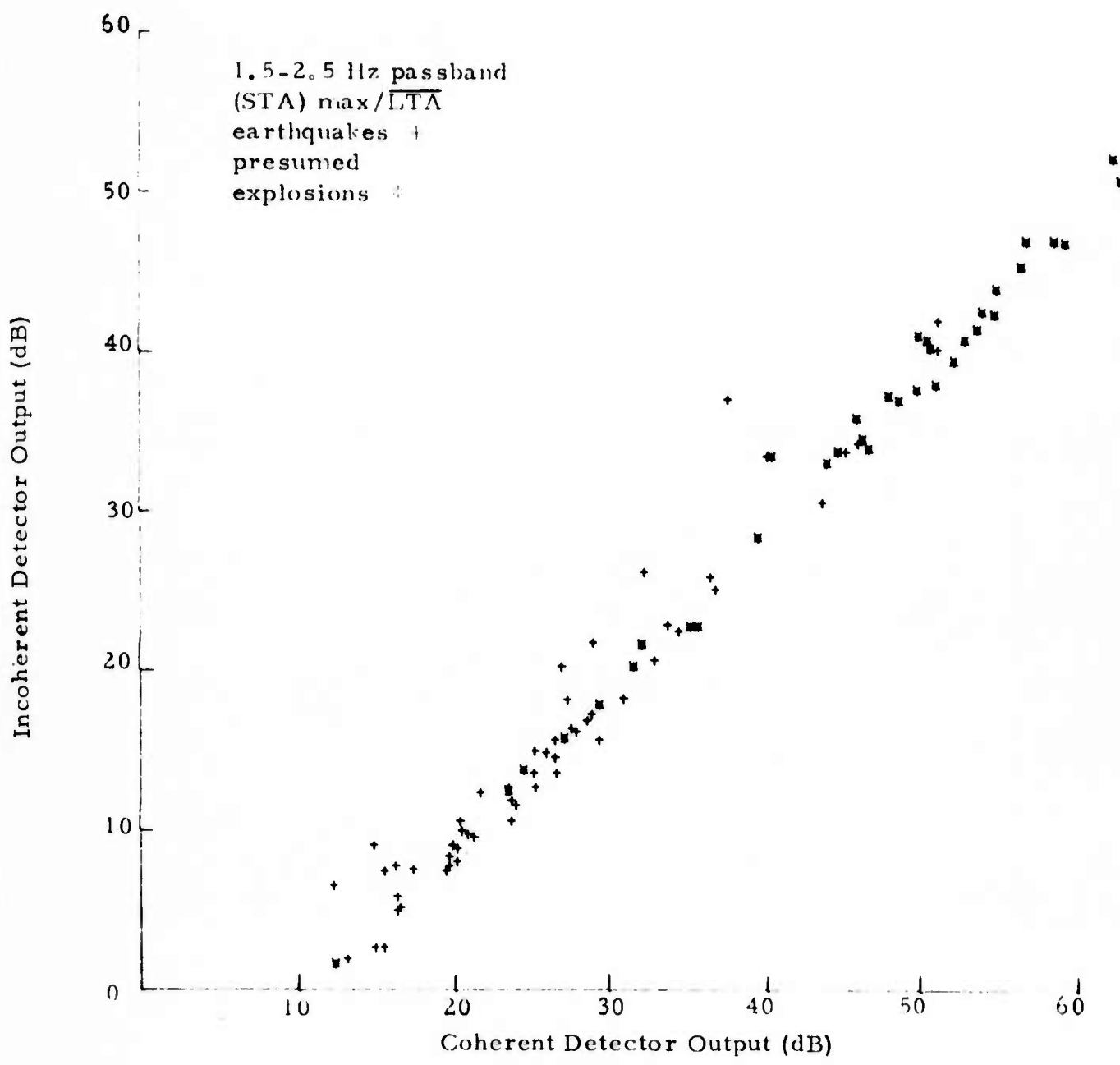


FIGURE IV-16
COHERENT ADJUSTED-DELAY DETECTOR OUTPUT VERSUS
INCOHERENT DETECTOR OUTPUT
($(STA)_{max}/LTA$ IN THE 1.5-2.5 Hz PASSBAND)

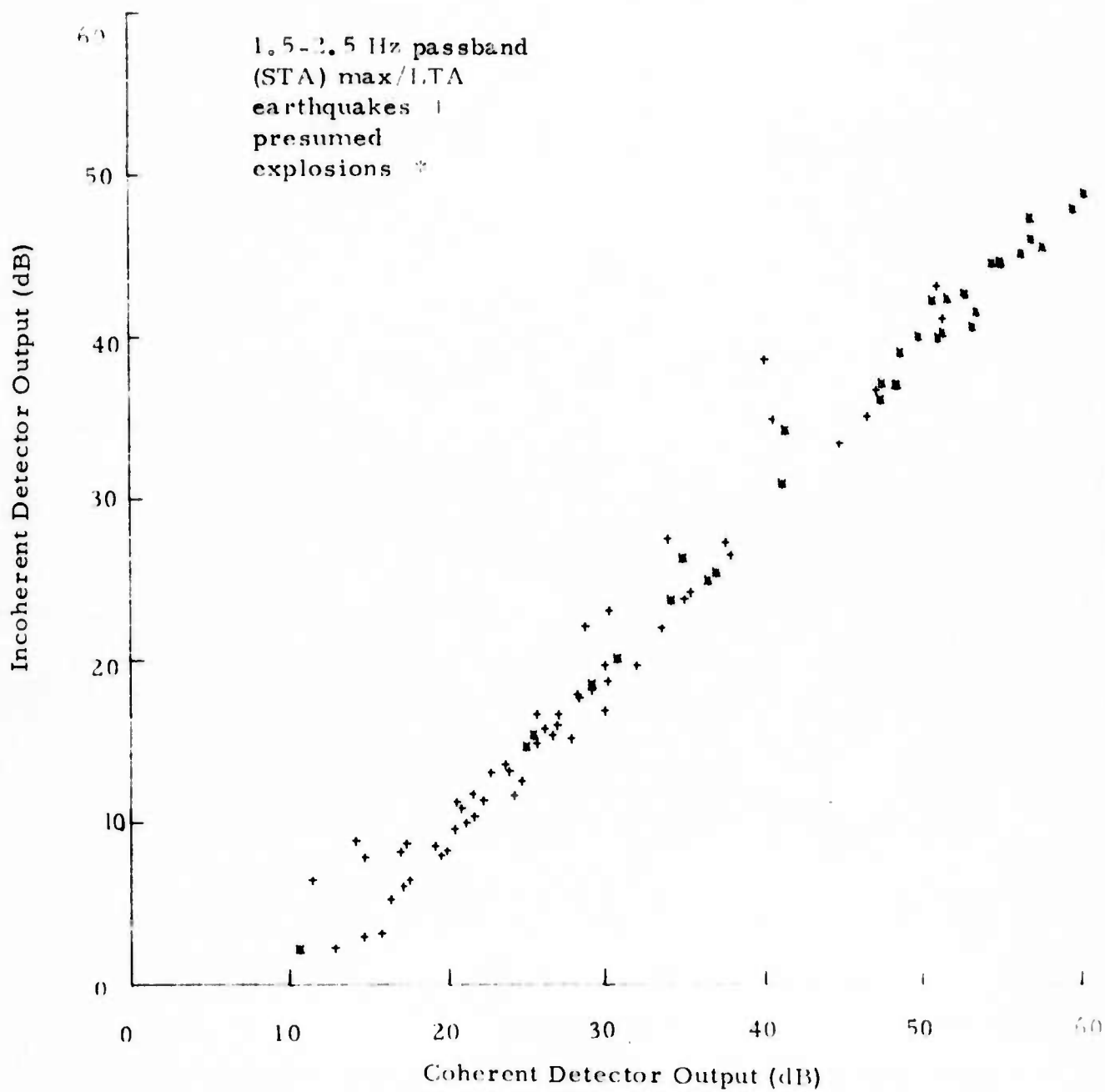
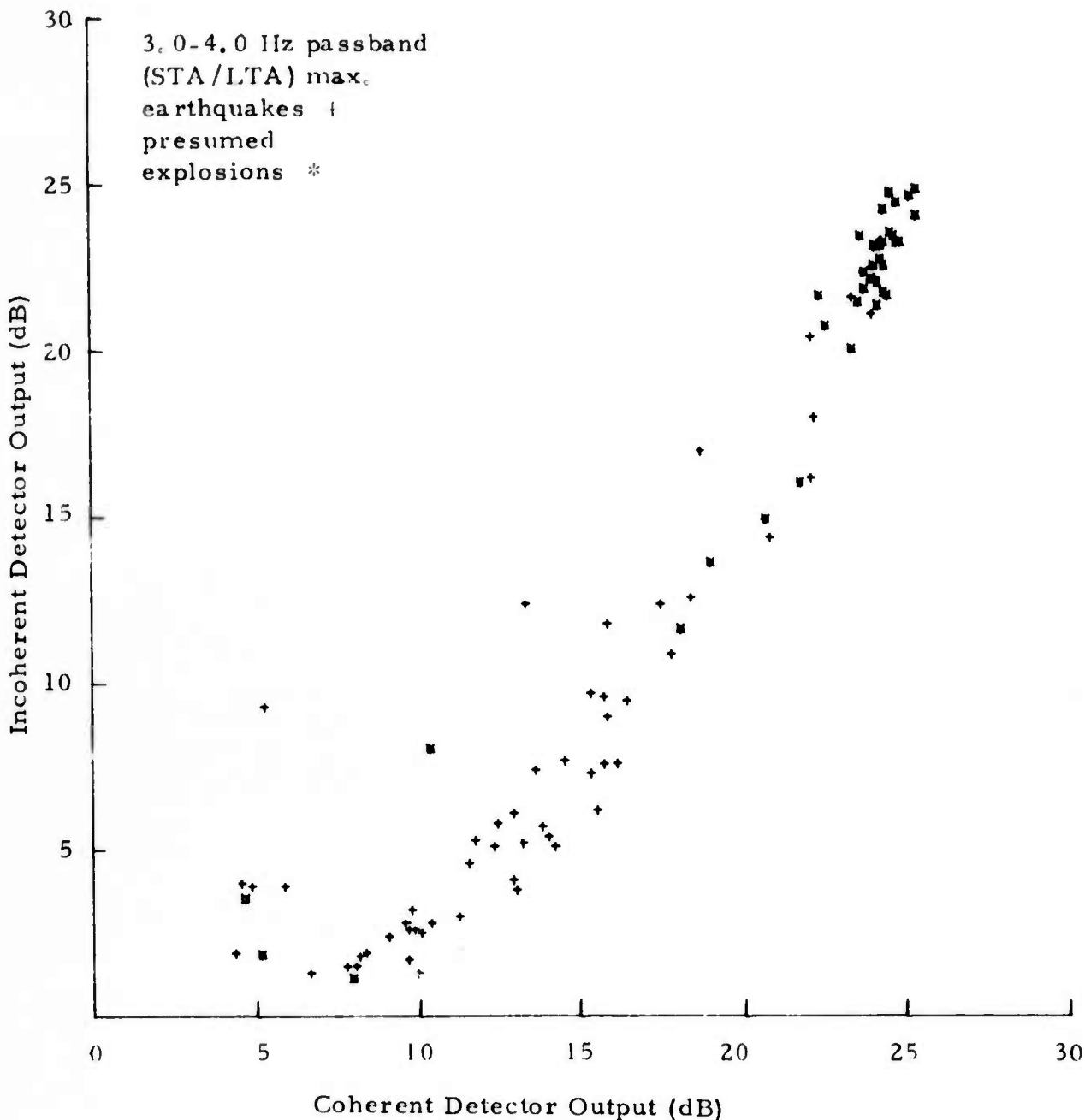


FIGURE IV-17
COHERENT DIVERSITY-STACK DETECTOR OUTPUT VERSUS
INCOHERENT DETECTOR OUTPUT
((STA)_{max}/LTA IN THE 1.5-2.5 Hz PASSBAND)



COHERENT ADJUSTED-DELAY DETECTOR OUTPUT VERSUS
 INCOHERENT DETECTOR OUTPUT
 $((STA/LTA)_{max})$ IN THE 3.0-4.0 Hz PASSBAND)

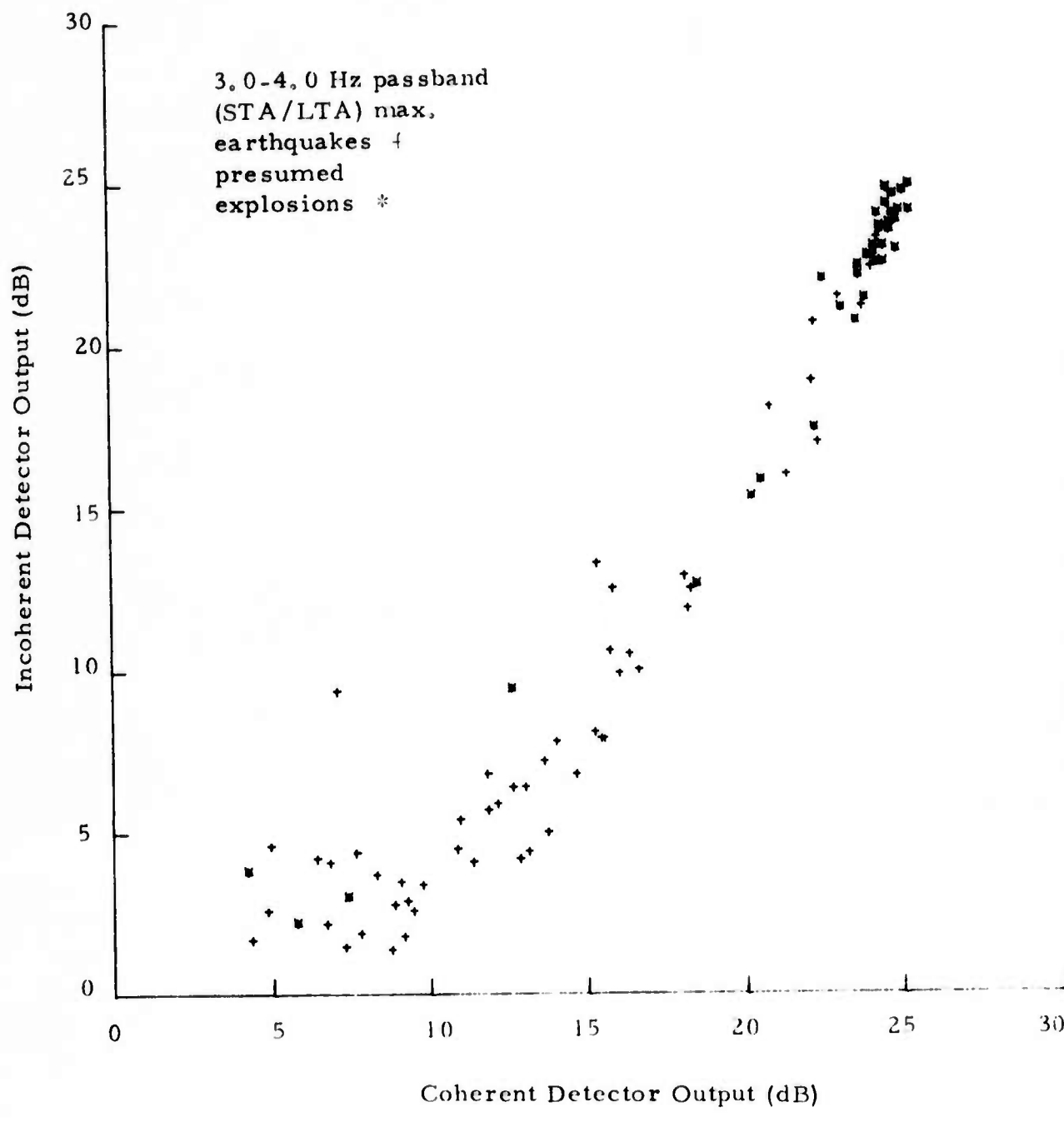


FIGURE IV-19

COHERENT DIVERSITY-STACK DETECTOR OUTPUT VERSUS
INCOHERENT DETECTOR OUTPUT
($(STA/LTA)_{max}$ IN THE 3.0-4.0 Hz PASSBAND)

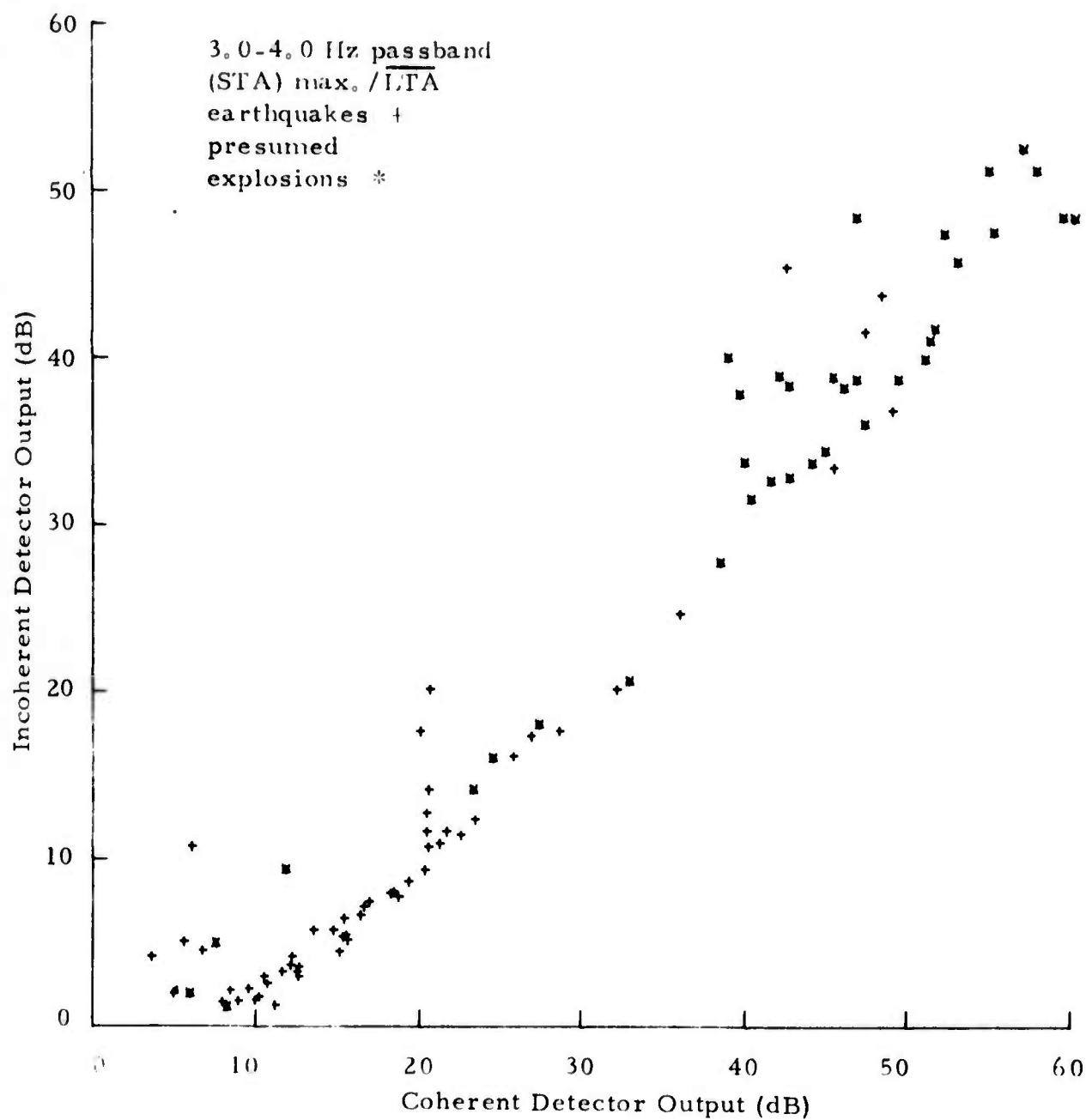


FIGURE IV-20
COHERENT ADJUSTED-DELAY DETECTOR OUTPUT VERSUS
INCOHERENT DETECTOR OUTPUT
($(STA)_{\max} / LTA$ IN THE 3.0-4.0 Hz PASSBAND)

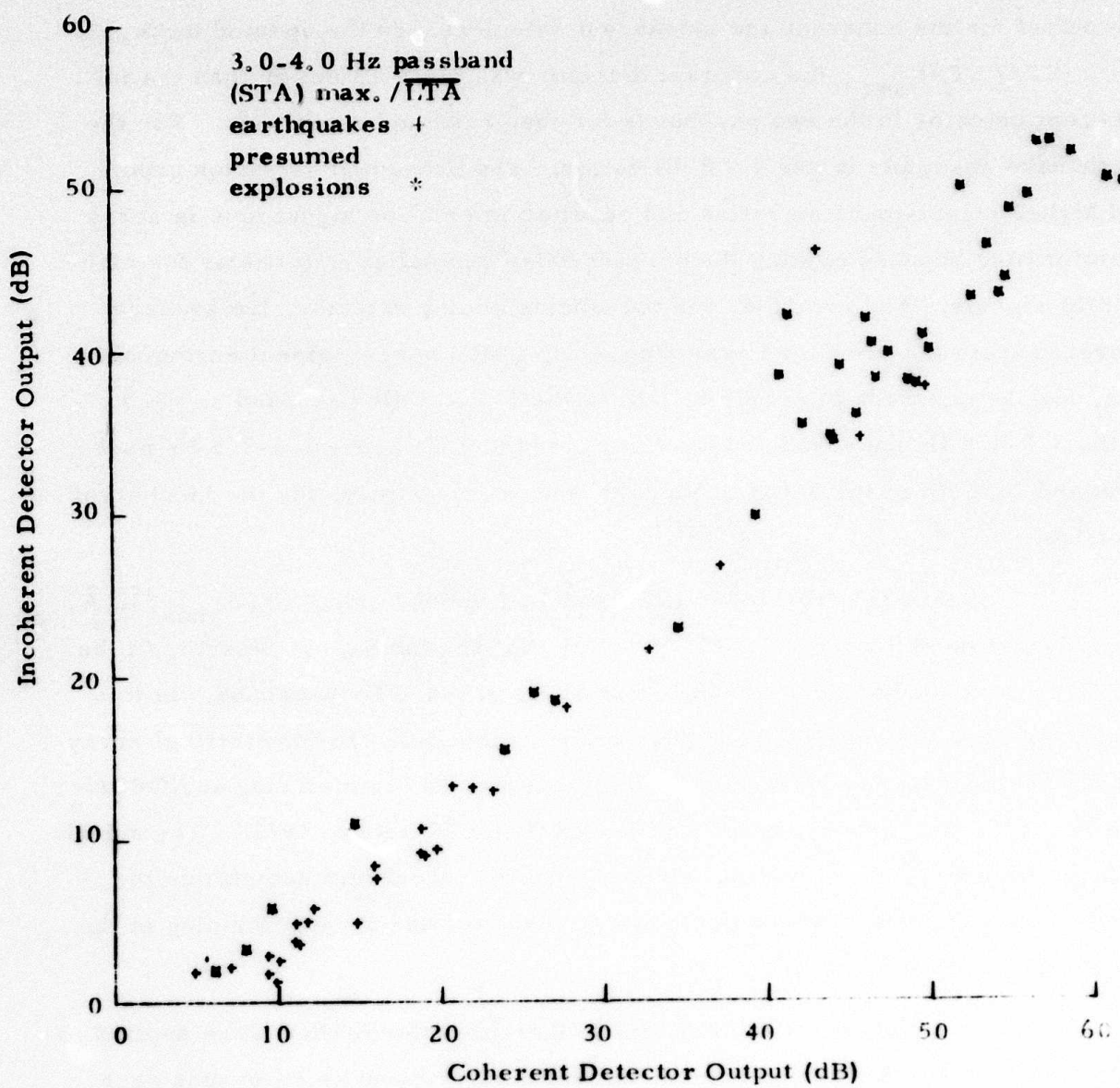


FIGURE IV-21
COHERENT DIVERSITY-STACK DETECTOR OUTPUT VERSUS
((STA)_{max} / LTA IN THE 3.0-4.0 Hz PASSBAND)

To summarize the detector outputs, Table IV-2 shows the average output for the coherent and incoherent detectors. In the updated mode, i.e., $(STA/LTA)_{max}$, the coherent detector was 2 - 3 dB better than the incoherent detector in the two passbands for the presumed explosions. For the earthquake ensemble it was 5 - 6 dB better. The presumed explosion group had higher signal-to-noise ratios and resulted in smaller signal loss in array beamforming because picking the correct delay anomalies was easier for higher SNR signals. For example, for the adjusted delay detector, the average decrease from the presumed explosion group to the near-regional earthquakes was, for the coherent detector, 6.2 dB in the 1.5-2.5 Hz passband and 8.3 dB in the 3.0-4.0 Hz passband, respectively, and 9.9 dB in the 1.5-2.5 Hz passband and 12.0 dB in the 3.0-4.0 Hz passband, respectively, for the incoherent detector.

For the frozen and averaged LTA mode, using $(STA)_{max}/\overline{LTA}$, the coherent detector was 10 - 11 dB better than the incoherent detector in the 1.5-2.5 Hz passband and 7 - 8 dB better in the 3.0-4.0 Hz passband. In this mode, the SNR estimate is more physically meaningful. The theoretical array gain for 22 channels is 13.4 dB and the signal loss in beamforming at NORSAR was about 3 - 4 dB in the signal band (Ringdal and Whitelaw, 1973). The smaller improvement of the coherent detector over the incoherent detector in the 3.0-4.0 Hz passband reflects the higher signal loss due to beamforming in the higher frequency passband.

Envelope detectors using Hilbert transformation were applied to four events - two presumed explosions and two earthquakes. Because each data point $E(t)$ in either the coherent or the incoherent beamforming process represents an independent estimate of amplitude, the theoretical maximum increase from STA-envelope detectors for coherent beamforming design would be about 11.8 dB. Table IV-3 lists the detector output for this method. The increased output from the STA method ranged from 0.5 dB to 11.3 dB for the

TABLE IV-2
AVERAGES OF DETECTOR OUTPUT FOR EVENT ENSEMBLE

Ensembles	Beams	Passband (Hz)	Coherent Beamforming		Incoherent Beamforming	
			$\left(\frac{STA}{LTA}\right)_{max}$	$\frac{(STA)_{max}}{LTA}$	$\left(\frac{STA}{LTA}\right)_{max}$	$\frac{(STA)_{max}}{LTA}$
36 events of presumed explosions	Adjusted Delay	1.5-2.5 3.0-4.0	23.7 21.9	45.8 41.4	21.0 19.8	34.7 34.1
	Diversity Stack	1.5-2.5 3.0-4.0	23.9 22.1	47.4 43.2	21.8 20.4	36.8 35.9
	Adjusted Delay	1.5-2.5 3.0-4.0	17.5 13.6	26.3 18.9	11.1 7.8	15.8 10.9
55 events of earthquakes	Diversity Stack	1.5-2.5 3.0-4.0	17.7 13.4	27.0 18.7	11.8 8.2	16.9 11.5
	Adjusted Delay	1.5-2.5 3.0-4.0	19.9 16.9	34.0 27.8	15.0 12.5	23.3 20.8
	Diversity Stack	1.5-2.5 3.0-4.0	20.2 16.8	35.1 28.4	15.7 13.0	24.8 21.2
Averages of 91 events						

TABLE IV-3
DETECTOR OUTPUT USING HILBERT TRANSFORMATION

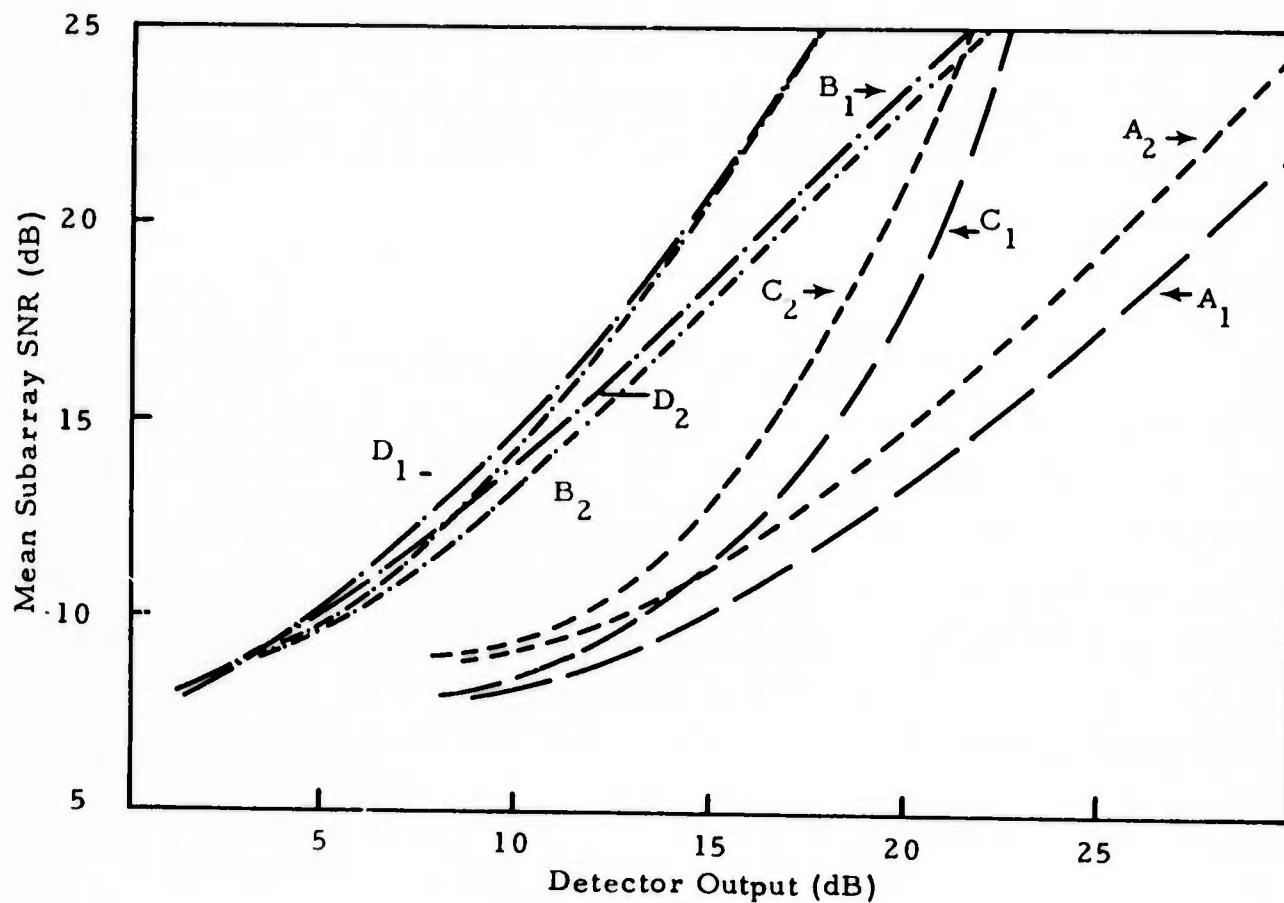
Events	Passband	Coherent Beamforming				Incoherent Beamforming			
		(STA/LTA)max (dB)	(STA/LTA) Adjusted Diversity Stack	(STA/LTA) Adjusted Delay	(STA/LTA) max/ STA (dB)	(STA/LTA) max (dB)	(STA/LTA) Adjusted Diversity Stack	(STA/LTA) max/ STA (dB)	(STA/LTA) max/ STA (dB)
WRS/248/07N	1.5~2.5 3.0~4.0	31.1 29.9	32.1 29.9	48.4 48.1	49.5 48.1	24.3 24.4	26.4 24.8	36.2 35.8	38.6 36.6
SWR/205/11N	1.5~2.5 3.0~4.0	17.3 18.5	17.8 17.8	22.3 21.0	22.5 20.3	8.5 9.0	8.9 9.6	11.7 11.8	12.5 12.5
WRS/277/10N	1.5~2.5 3.0~4.0	29.9 30.3	30.3 30.6	46.1 50.5	47.0 50.6	26.1 26.7	26.8 27.2	34.1 39.1	35.6 40.1
KAZ/282/06N	1.5~2.5 3.0~4.0	35.8 33.4	36.4 33.6	51.8 52.9	53.8 54.9	30.2 29.2	32.2 30.2	38.5 40.0	41.5 42.4

coherent detector and from 0.5 dB to 8.6 dB for the incoherent detector. The average increase was 7.3 dB and 4.1 dB for the $(STA/LTA)_{max}$ and $(STA)_{max}/\overline{LTA}$ modes, respectively, with the coherent diversity-stack detector and 5.1 dB and 2.1 dB for the $(STA/LTA)_{max}$ and $(STA)_{max}/\overline{LTA}$ modes with the incoherent diversity-stack detector. Thus the operational mode detector registered a more significant increase than the frozen and averaged LTA mode detector.

2. A Simulation Study

In order to determine the detector performance at different event magnitudes, a simulation study was conducted by burying a signal scaled over a range of amplitudes in subarray beams of noise and subsequently generating the coherent and incoherent beams for the detection system. The subarray beam amplitudes were obtained by computing the ratio of the signal peak amplitude to the noise RMS value for each subarray and averaging the ratios over the full array. These ratios, which are expressed in decibels, are called the subarray SNR's.

Figure IV-22 shows the detector output versus the mean subarray signal-to-noise ratio for the presumed explosion KAZ/282/06N. Curves A_1 and A_2 are for the frozen and averaged long-term average mode, i.e., $(STA)_{max}/\overline{LTA}$, of coherent detector operating in the 1.5-2.5 Hz and 3.0-4.0 Hz passbands, respectively. Curves B_1 and B_2 are for the $(STA)_{max}/\overline{LTA}$ mode of incoherent detector output in the 1.5-2.5 Hz and 3.0-4.0 Hz passbands, respectively. Curves C_1 and C_2 are for the updated long-term average mode, i.e., $(STA/LTA)_{max}$, of the coherent detector output in the 1.5-2.5 Hz and 3.0-4.0 Hz passbands, respectively, while curves D_1 and D_2 are for the updated LTA mode of incoherent detector in the 1.5-2.5 Hz and 3.0-4.0 Hz passbands, respectively.



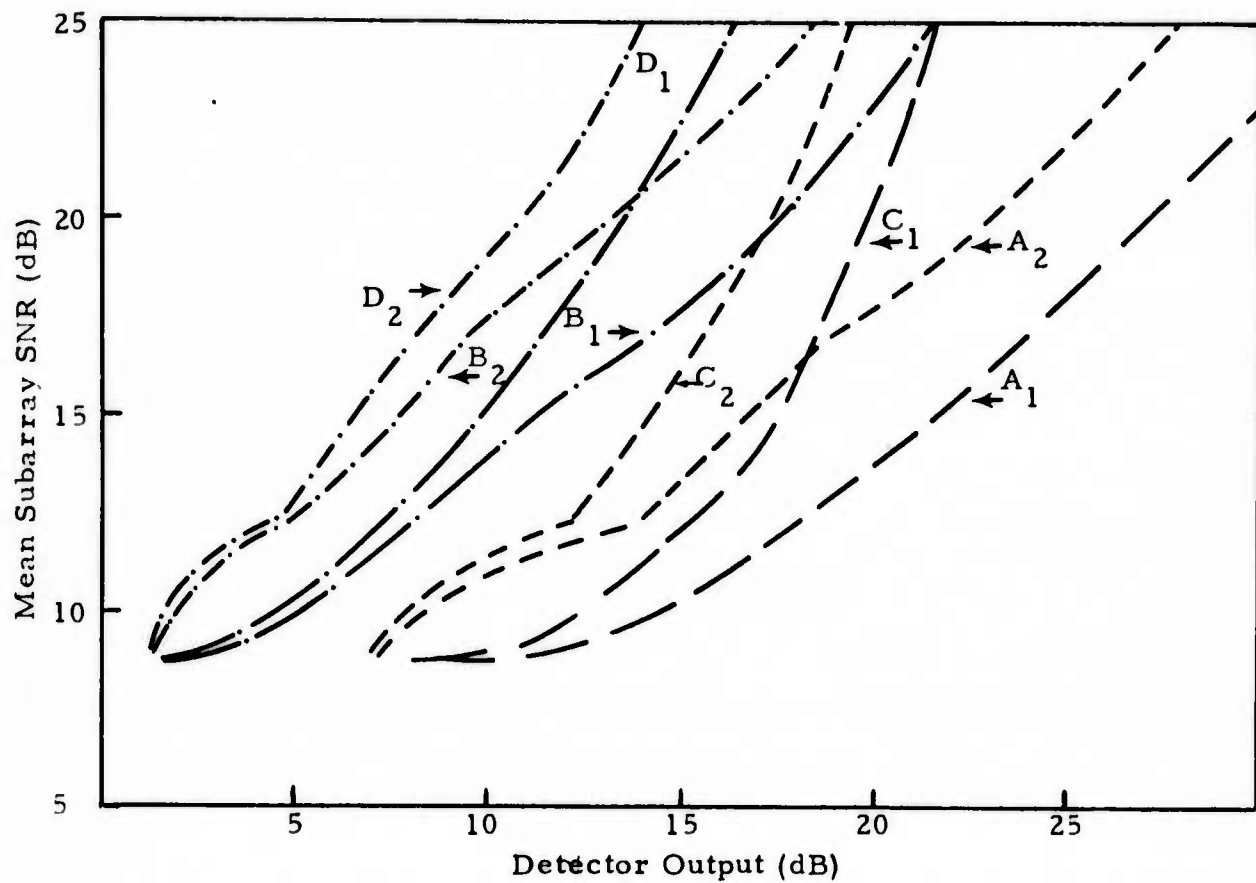
Coherent :	A_1, C_1 (1.5-2.5 Hz)
	A_2, C_2 (3.0-4.0 Hz)
Incoherent:	B_1, D_1 (1.5-2.5 Hz)
	B_2, D_2 (3.0-4.0 Hz)
(A, B: $(STA)_{max} / \overline{LTA}$ Mode)	
(C, D: $(STA / LTA)_{max}$ Mode)	

FIGURE IV-22
MEAN SUBARRAY SNR VERSUS DETECTOR OUTPUT
(KAZ/282/06N)

For a given mean subarray SNR, the incoherent detector performed better in the 3.0-4.0 Hz passband while the reverse was true for the coherent detector. This reflects the fact that the signal loss was higher in the 3.0-4.0 Hz passband than in the 1.5-2.5 Hz passband for the coherent detector. Typical SNR detection thresholds used at NORSAR are 11 dB for the coherent detector and 4 dB for the incoherent detector (Ringdal et al., 1972). Using these levels as the basis for defining the false alarm rates in order to compare the detector's performance, then, as the mean SNR decreases, the detector output reaches these levels in the order: curves C_2 , D_1 , B_1 , A_2 , D_2 , B_2 , C_1 , and A_1 . Direct interpretation of this order suggests that curve A_1 , the $(STA)_{max}/LTA$ mode of coherent detector operating in the 1.5-2.5 Hz passband, yields best performance and the $(STA/LTA)_{max}$ mode of coherent detector operating in the 3.0-4.0 Hz passband ranks last in performance.

For the overall performance of the two groups of curves, the incoherent detector has better performance than the coherent detector in the 3.0-4.0 Hz passband, but not in the 1.5-2.5 Hz passband. Also, for a given mean SNR, the difference in detector output between the two passbands is about 2 dB for the coherent detector, and is less than 1 dB for the incoherent detector.

Figure IV-23 shows the results of the same simulation study for the event WRS/248/07N, which was 11.9 degrees away and 7 km deep. Curves A_1 , A_2 , B_1 , B_2 , C_1 , C_2 , D_1 , and D_2 correspond to the same cases as in Figure IV-22. One of the most striking features for this event was clear superiority of detector performance in the 1.5-2.5 Hz passband. The lower detector output in the 3.0-4.0 Hz passband than in the 1.5-2.5 Hz passband can be attributed to better noise coherency in the 3.0-4.0 Hz passband within a subarray and noise incoherency between the subarrays. Evaluating the detector performance on the basis of the detection thresholds used at NORSAR, as the incoming signal becomes weaker, the detector output reaches those threshold



Coherent :	A ₁ , C ₁ (1.5-2.5 Hz)
	A ₂ , C ₂ (3.0-4.0 Hz)
Incoherent:	B ₁ , D ₂ (1.5-2.5 Hz)
	B ₂ , D ₂ (3.0-4.0 Hz)
(A, B: (STA) _{max} / LTA Mode)	
(C, D: (STA/L TA) _{max} Mode)	

FIGURE IV-23
MEAN SUBARRAY SNR VERSUS DETECTOR OUTPUT
(WRS/248/07N)

levels in the order: curves D_2 , C_2 , B_2 , A_2 , D_1 , B_1 , C_1 , and A_1 . Since the coherent and incoherent detectors in the 1.5-2.5 Hz passband have 11 dB and 4 dB output, respectively, at the 9 dB level of mean subarray SNR, the above order is not sufficiently significant to resolve the difference in performance of the detectors.

In general, the event KAZ/282/06N has better signal similarity than the event WRS/248/07N because the former event, a presumed explosion, yields higher detector output than the latter, an earthquake, at the same level of mean subarray SNR. The presumed explosion showed more energy in the 3.0-4.0 Hz passband than the earthquake event as well as higher signal coherency.

3. The Measured Detection Probability

Figures IV-24 through IV-27 show the measured detection probability from the ensemble of 91 events for various cases. Figures IV-24 and IV-25 are for the updated LTA mode, using $(STA/LTA)_{max}$, in the 1.5-2.5 Hz and 3.0-4.0 Hz passbands, respectively, and Figures IV-26 and IV-27 for the frozen and averaged LTA mode, using $(STA)_{max}/\overline{LTA}$, in the same two passbands.

For a given decision threshold, the diversity-stack beams show a higher detection probability, particularly for the incoherent detectors. However, for weaker signals the differences between the adjusted-delay and the diversity-stack beams are smaller because the signal amplitudes are comparable to the noise level and thus the channel weights are more random.

The detection probability is highly dependent upon the distribution of signal amplitude involved. As mentioned earlier, the event selection was constrained to the NORSAR near-regional earthquakes and the presumed explosions available on the existing NORSAR short-period subarray beam tapes. The bodywave magnitudes were not uniformly distributed for these data because

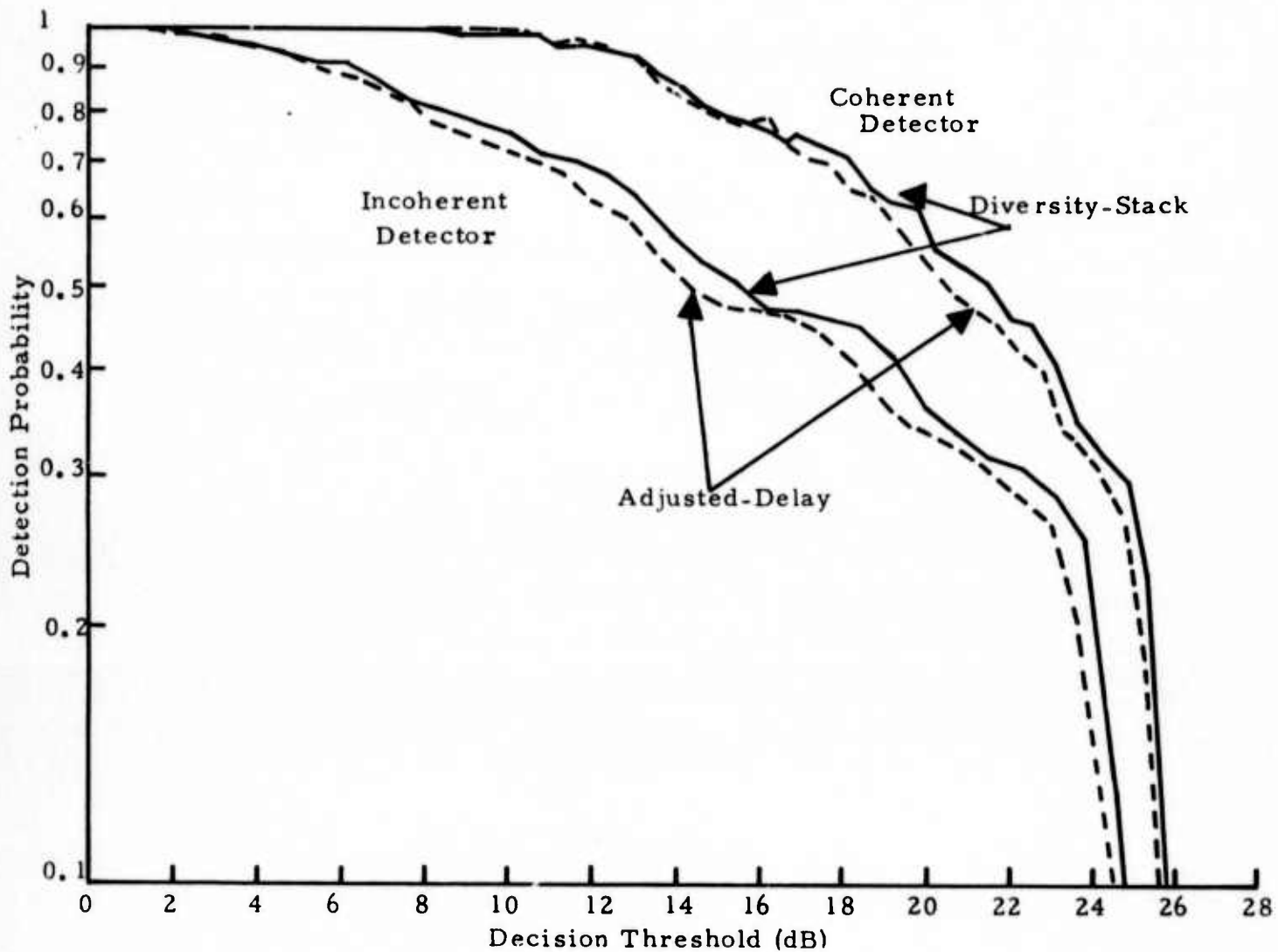


FIGURE IV-24
DETECTION PROBABILITY FROM 91 EVENTS
(STA/LTA)_{max} IN 1.5-2.5 Hz PASSBAND

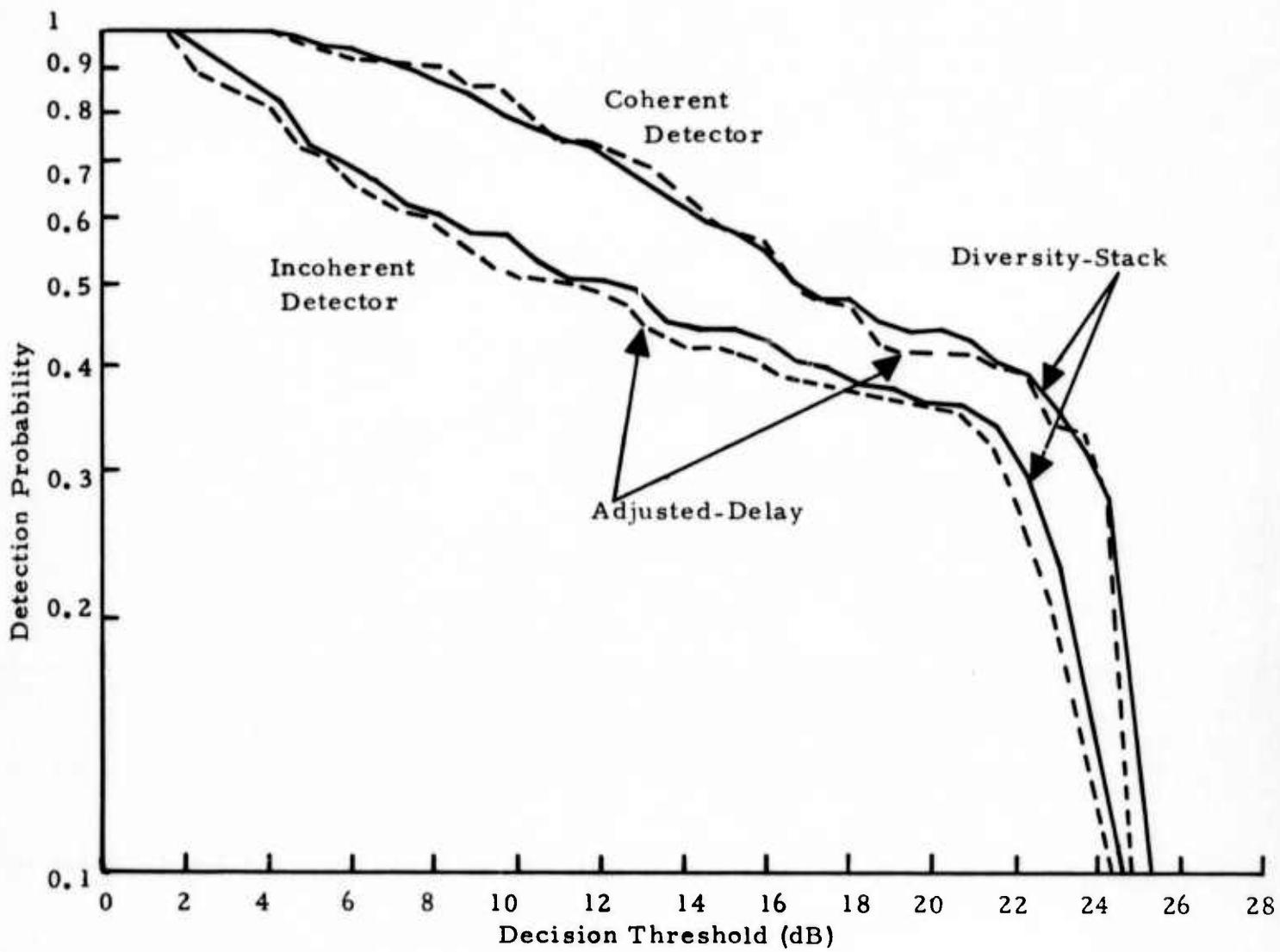


FIGURE IV-25
DETECTION PROBABILITY FROM 91 EVENTS
 $(STA / LTA)_{max}$ IN 3.0-4.0 Hz PASSBAND

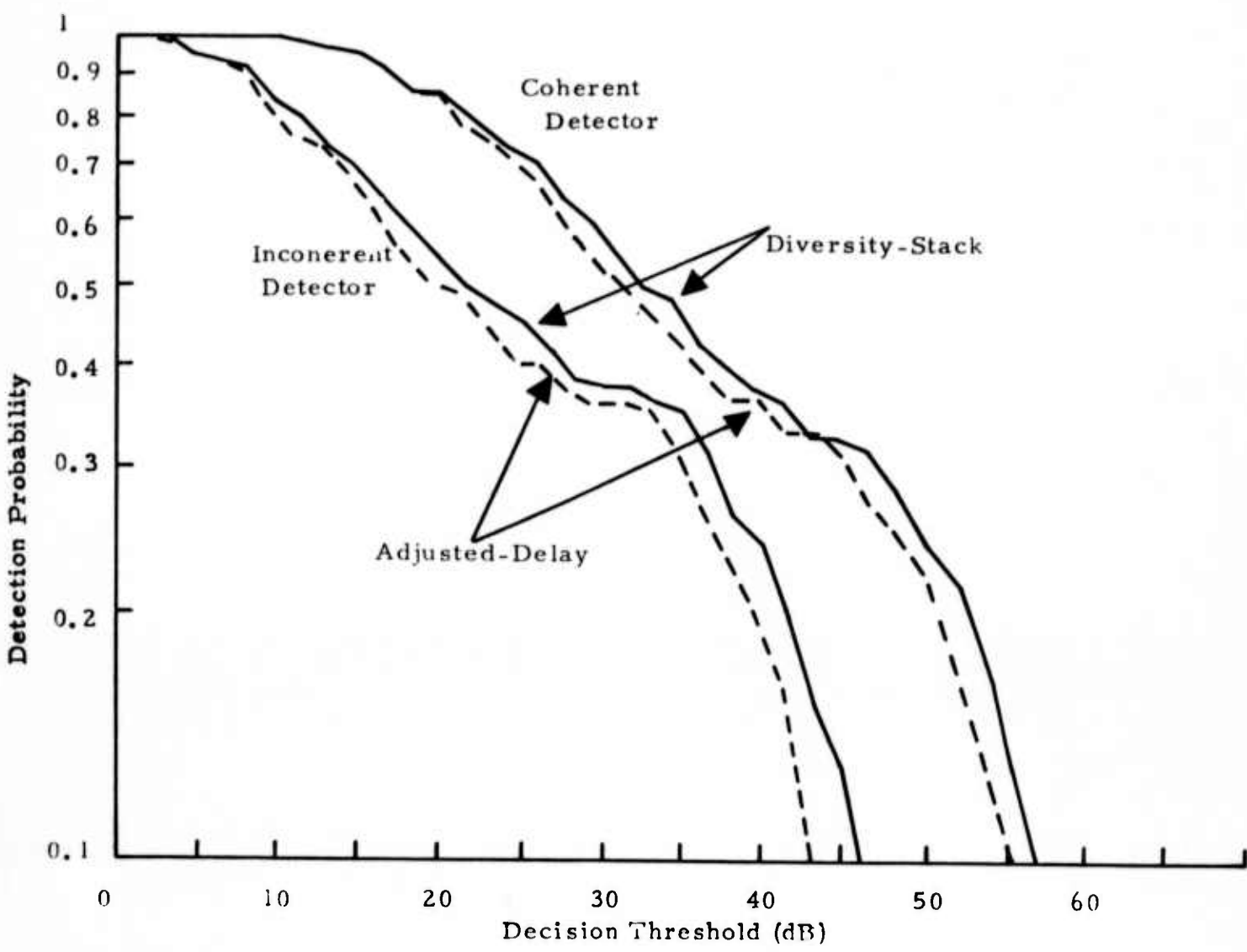


FIGURE IV-26
DETECTION PROBABILITY FROM 91 EVENTS
 $(STA)_{max}/\overline{LTA}$ IN 1.5-2.5 Hz PASSBAND

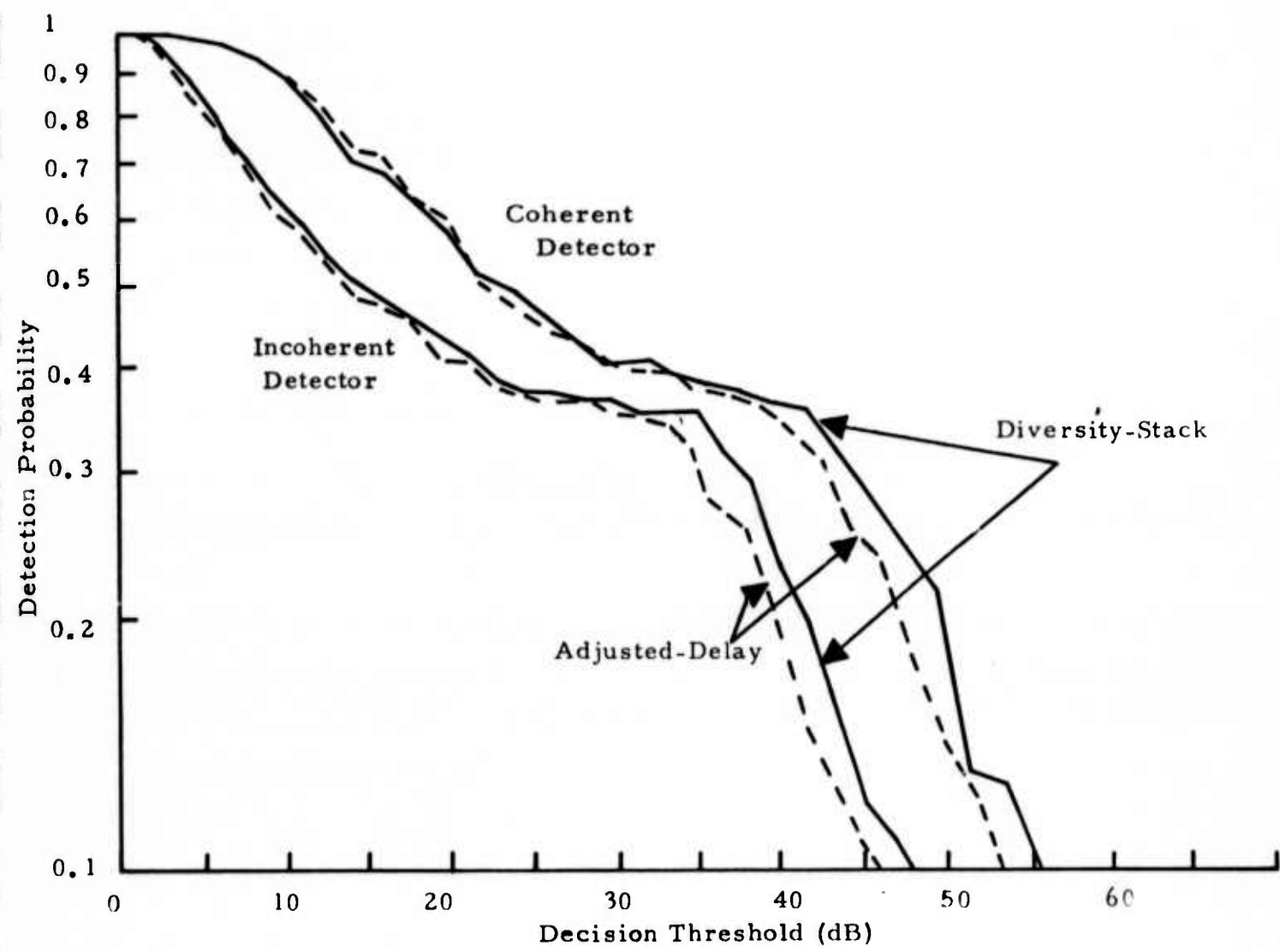


FIGURE IV-27
DETECTION PROBABILITY FROM 91 EVENTS
 $(STA)_{max}/\overline{LTA}$ IN 3.0-4.0 Hz PASSBAND

the 36 presumed explosions were of larger magnitude and generally had stronger P-waves (see Table III-2). The resulting probability curves for both the coherent and incoherent detectors are significantly affected by these strong events, particularly for decision thresholds greater than 18 dB and 36 dB levels for the updated and frozen LTA modes, respectively.

In brief, the diversity-stack beams yield higher detection probability for both coherent and incoherent detectors as generally expected. The next subsection presents the evaluation of these detectors on the basis of their operating characteristic curves.

E. THE MEASURED DETECTOR OPERATING CHARACTERISTICS

In this subsection the false alarm rate and detection probability measurements are combined together to form the detector operating characteristics or operating curves for constant detector output. The conventional evaluation of detector performance can be accomplished by appraising these characteristics. In the last two subsections, it has been shown that the diversity-stack beams outperform the adjusted-delay beams for signal detection and have more uniform false alarm probability distribution than the adjusted delay beams for both coherent and incoherent detectors. Consequently, the operating curves are formed for the diversity-stack beams only.

Figures IV-12 and IV-13 (False Alarm Probability for Diversity-Stack Beams) and Figures IV-24 to IV-27 (Detection Probability for Diversity-Stack Beams) indicate that the overlapping range of the actual detector output is not sufficiently large enough to form the characteristic functions by eliminating the constant detector output (signal-to-noise ratio in dB) because the events used in this study usually have strong signals and the detector output in noise is very low. One way to surmount this difficulty is to extrapolate

the false alarm probability curves in Figures IV-12 and IV-13 to the higher thresholds sufficiently high enough to form the operating curves with the detection probabilities in Figures IV-24 to IV-27. The parameters of Gaussian distribution functions, mean values and standard deviations, for the observed false alarm probabilities in Subsection IV-C can be used for this purpose. For the probabilities less than 10^{-6} of normal distribution functions, the mathematical handbook compiled by Abramowitz and Stegun (1966) can serve as a good aid for approximate computation.

Figure IV-28 shows the operating characteristics for the updated LTA mode, using $(STA/LTA)_{max}$ for the coherent and incoherent detectors in the 1.5-2.5 Hz and 3.0-4.0 Hz passbands, respectively. The false alarm probabilities have been extrapolated to the 10^{-9} levels (17.5 dB and 15.8 dB for the coherent detector in the 1.5-2.5 Hz and 3.0-4.0 Hz passbands, respectively, and 4.7 dB and 5.6 dB for the incoherent detector in the 1.5-2.5 Hz and 3.0-4.0 Hz passbands, respectively) and are plotted in logarithms while the detection probabilities are shown in linear scale. For the same level of false alarm probabilities, the detector performance is ranked in the order: incoherent detector operating in the 1.5-2.5 Hz passband, coherent detector in the 1.5-2.5 Hz passband, incoherent detector in the 3.0-4.0 Hz passband and coherent detector in the 3.0-4.0 Hz passband. This fact means that the incoherent detectors outperform the coherent detectors for each passband and it is more pronounced in the range of low false alarm rate because the long-term-average, LTA, for the incoherent beam increases slower than the coherent beam for the $(STA/LTA)_{max}$ mode of detectors after the onset of signal arrivals. For the weak-signal range, it still clearly remains true that the incoherent detector yields better performance than the coherent detector for the updated LTA mode which is the "Operational" mode at NORSAR on-line detection system.

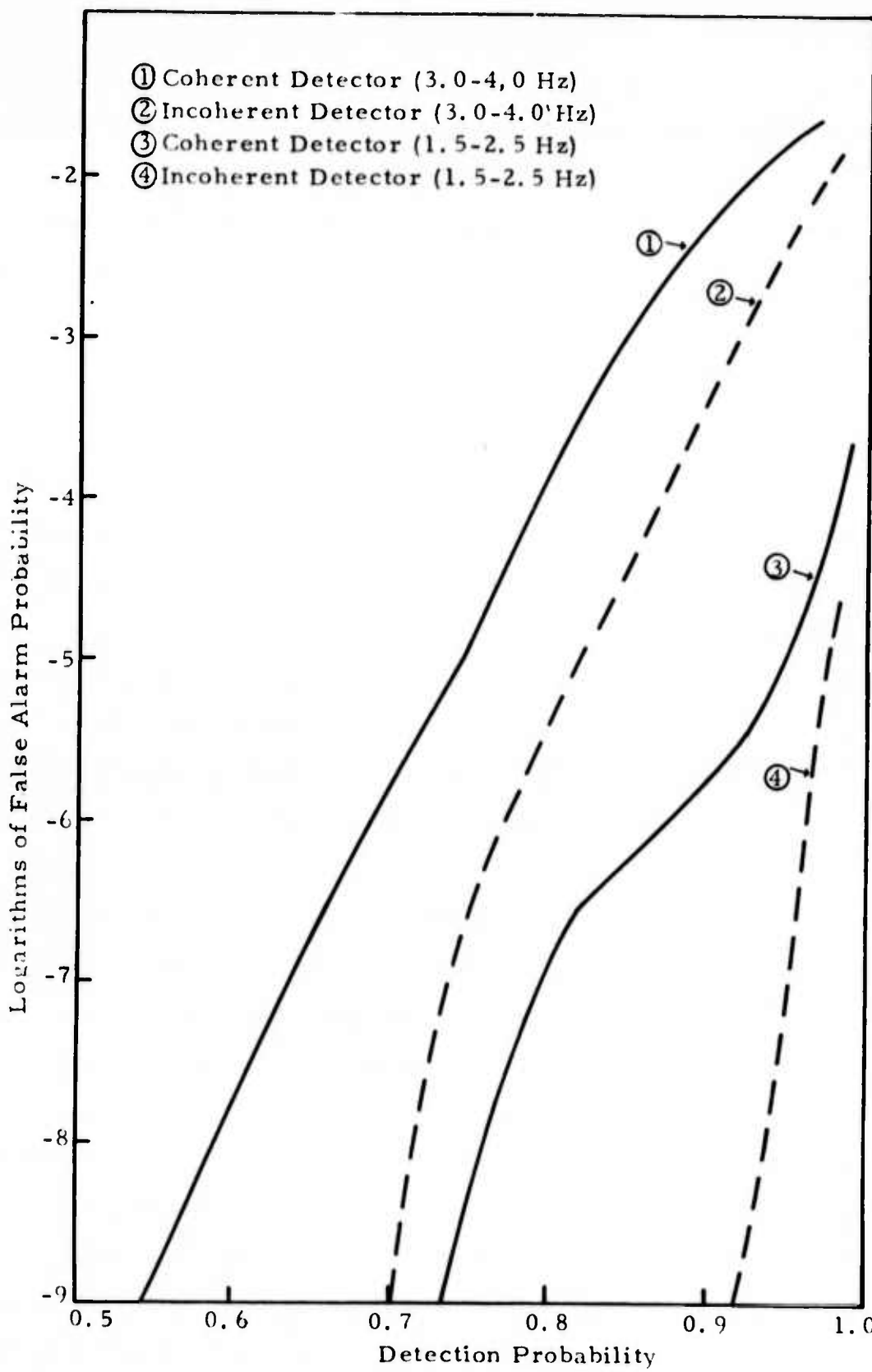


FIGURE IV-28

DETECTOR OPERATING CHARACTERISTICS
(DIVERSITY - STACK BEAMS (STA/LTA)_{max} MODE)

Figure IV-29 shows the detector operating characteristics for the frozen and averaged LTA mode, using $(STA)_{max} / \overline{LTA}$, for the diversity-stack beams in the 1.5-2.5 Hz and 3.0-4.0 Hz passbands. For the strong signal range and low false alarm rate level, the incoherent detector clearly demonstrates the superior performance over the coherent detector in both passbands. For the 3.0-4.0 Hz passband, the coherent and incoherent detectors yield about the same performance with slight indication of incoherent detector being better than the coherent detector. However, for the 1.5-2.5 Hz passband, both coherent and incoherent detectors show the same performance for the present ensemble of events. Finer resolution of detection probability in the weak-event range might tell the difference.

In summary, from the evaluation of detector operating characteristics, it is concluded that the incoherent detector operating in the 1.5-2.5 Hz passband yields best performance and the coherent detector in the 3.0-4.0 Hz passband the worse among the four cases studied. For each passband, the incoherent detector shows the better performance than the coherent detector. For detecting the underground explosions and near-regional earthquakes, the incoherent detector is superior to the coherent detector.

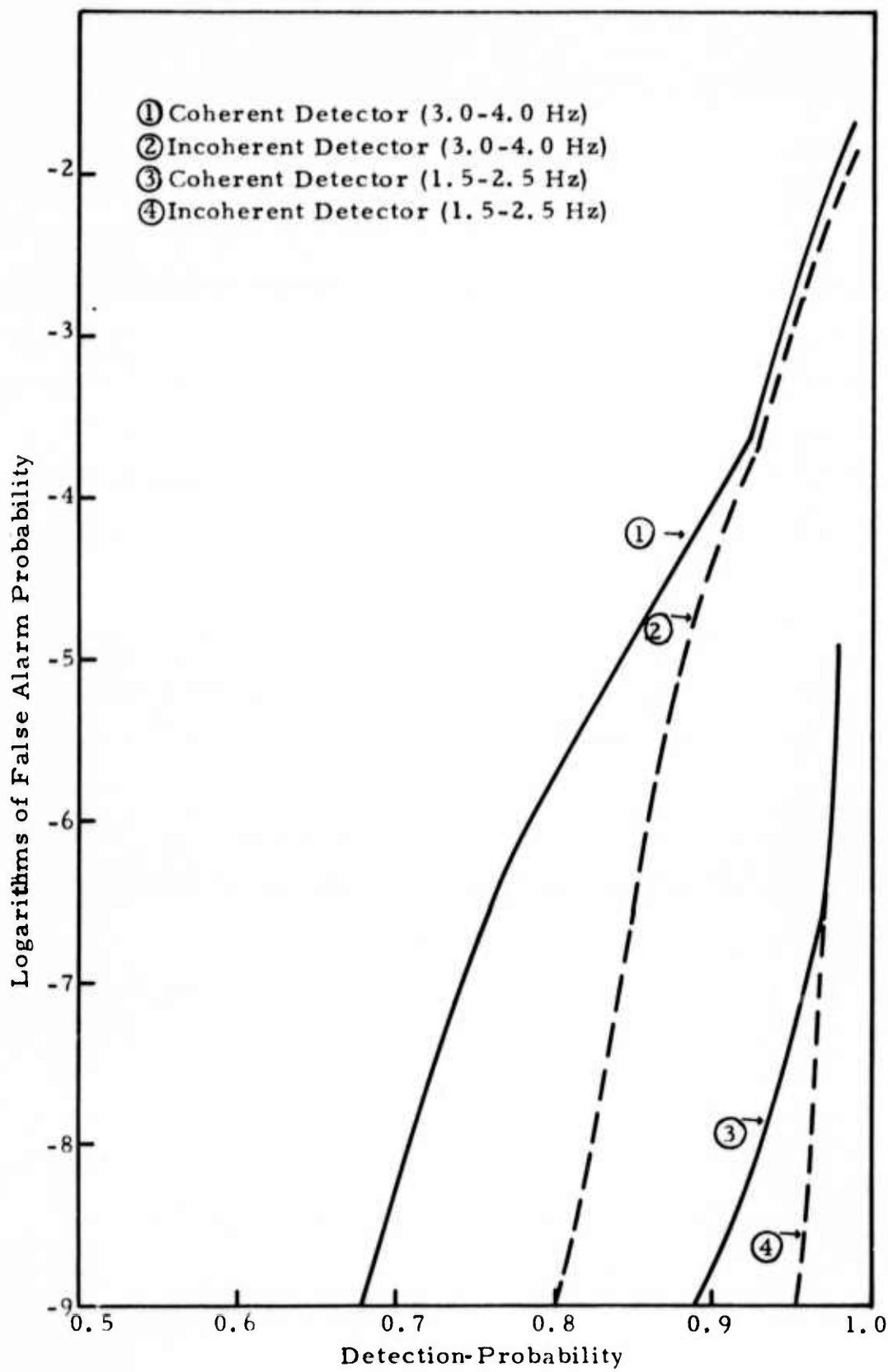


FIGURE IV-29

DETECTOR OPERATING CHARACTERISTICS
(DIVERSITY-STACK BEAMS (STA)_{max}/LTA MODE)

SECTION V CONCLUSIONS

This section summarizes the major results and conclusions of this study.

A. FALSE ALARM RATE MEASUREMENTS

- The false alarm probability density function from either the coherent or the incoherent detector output closely follows a Gaussian distribution. This indicates that the amplitude distribution of the envelope of the noise beam can be modeled by a lognormal distribution.
- For the coherent envelope detector, the 1.5-2.5 Hz passband had a higher false alarm probability than the 3.0-4.0 Hz passband for a given decision threshold.
- For the incoherent detector, the opposite is true. For a given decision threshold, the 3.0-4.0 Hz passband had a higher false alarm probability than the 1.5-2.5 Hz passband.
- The detectors using true envelopes computed with Hilbert-transform yielded higher false alarms than the STA-envelope detectors because the former did not incorporate any smoothing through integration.
- In order to achieve the false alarm rates less than one/per beam/per day, the decision threshold for detection must be larger than 9 dB for the coherent detector in both passbands. For the incoherent detector, the thresholds are 3 dB in the 1.5-2.5 Hz

passband and 4.5 dB in the 3.0-4.0 Hz passband.

B. DETECTION PERFORMANCE

In this subsection, the concluding summary on detection is based only on the detector output for the presumed explosions and near-regional earthquakes without taking into account the detector's false alarm rates. Overall conclusions on relative detector performance are in Subsection V-C.

- For the operational mode detectors using a running STA/LTA ratio, the coherent detector output was 2-3 dB higher than the incoherent detector in both passbands for the presumed-explosion ensemble. For the earthquake ensemble, it was 5-6 dB higher.
- For the frozen-LTA-mode detectors using $(STA)_{max}/\overline{LTA}$, the coherent detector yielded a 10-11 dB higher output than the incoherent detector in the 1.5-2.5 Hz passband and 7-8 dB in the 3.0-4.0 Hz passband.
- The average detector output for diversity-stack beams using Hilbert transform pairs was 7.3 dB and 4.1 dB higher than the STA-envelope average for the $(STA/LTA)_{max}$ and $(STA)_{max}/\overline{LTA}$ coherent detectors, respectively, and 5.1 dB and 2.1 dB higher for the $(STA/LTA)_{max}$ and $(STA)_{max}/\overline{LTA}$ incoherent detectors, respectively, for four events.
- The simulation study where the scaled signal amplitudes were buried in noise suggested that the coherent detector operating in the 1.5-2.5 Hz passband yielded the best detection among the various detectors studied. However, for the 3.0-4.0 Hz passband the incoherent detector yielded better performance than the coherent detector.

- A detector where the LTA is delayed relative to the STA or E(t) envelope can reduce signal contamination in the LTA and thereby provide a better signal-to-noise ratio measurement.
- The diversity-stack beams had a higher detection probability than the adjusted-delay beams for both coherent and incoherent detectors.

C. DETECTOR OPERATING CHARACTERISTICS

Final conclusion on detector performance is summarized as follows:

- The incoherent detector yields better performance than the coherent detector in both the 1.5-2.5 Hz and the 3.0-4.0 Hz passbands.
- Both coherent and incoherent detectors yield better performance in the 1.5-2.5 Hz passband than in the 3.0-4.0 Hz passband.
- The envelope detector using Hilbert transformation operating at a given level produced a larger false alarm rate but an even better detection performance than the STA type of detector at the equivalent level. Thus the actual operating characteristic of the Hilbert transform envelope detector was superior to the STA envelope detector.

In conclusion, for detecting underground explosions and near-regional seismic signals at NORSAR, the incoherent beamforming envelope detector is superior to the coherent beamforming envelope detector, as expected. For teleseismic events, however, it may not be expected that the incoherent detector would still yield the better performance. Hence it is worthwhile to use the incoherent detector as a supplement to the coherent detector in order to maintain good detection performance for events at all distances.

SECTION VI
REFERENCES

- Abramowitz, M., and I. A. Stegun, 1966, Handbook of Mathematical Functions With Formulas, Graphs and Mathematical Tables, U.S. Department of Commerce.
- Barnard, T. E., and R. L. Whitelaw, 1972, Preliminary Evaluation of the Norwegian Short-Period Array, Special Report No. 6, AFTAC Contract Number F33657-71-C-0843, Texas Instruments Incorporated, Dallas, Texas.
- Bracewell, R., 1965, The Fourier Transform and Its Applications, p. 267, McGraw-Hill, New York, New York.
- Capon, J., 1972, Comparison of Short-Period Microseismic Noise at LASA and NORSAR, Lincoln Laboratory Report, MIT.
- Cizek, V., 1970, Discrete Hilbert Transform, IEEE Transactions on Audio and Electroacoustics, Volume AU-18.
- IBM, 1970, Interim NORSAR Signal and Noise Analysis, ESD-TR-72-122.
- Lacoss, R. T., 1972, Variations of False Alarm Rates at NORSAR, Lincoln Laboratory Report, MIT.
- Ringdal, F., E. S. Husebye, and A. Dahle, 1972, Event Detection Problems Using a Partially Coherent Seismic Array, NORSAR Technical Report 45.
- Ringdal, F., and R. L. Whitelaw, 1973, Continuous Evaluation of the Norwegian Short-Period Array, Special Report No. 9, AFTAC Contract Number F33657-72-C-0725, Texas Instruments Incorporated, Dallas, Texas.

Texas Instruments, Incorporated, 1971, Documentation of NORSAR Short-Period
Array Evaluation Software Package, AFTAC Contract Number F33657-
69-C-1063, Dallas, Texas.